

2013

## A Novel Resistance Exercise Machine for Use in a Lower Body Negative Pressure Box to Counteract the Effects of Weightlessness

Christine M. Dailey  
*Embry-Riddle Aeronautical University - Daytona Beach*

Follow this and additional works at: <https://commons.erau.edu/edt>



Part of the [Biomedical Engineering and Bioengineering Commons](#), and the [Mechanical Engineering Commons](#)

---

### Scholarly Commons Citation

Dailey, Christine M., "A Novel Resistance Exercise Machine for Use in a Lower Body Negative Pressure Box to Counteract the Effects of Weightlessness" (2013). *Dissertations and Theses*. 43.  
<https://commons.erau.edu/edt/43>

This Thesis - Open Access is brought to you for free and open access by Scholarly Commons. It has been accepted for inclusion in Dissertations and Theses by an authorized administrator of Scholarly Commons. For more information, please contact [commons@erau.edu](mailto:commons@erau.edu).

A Novel Resistance Exercise Machine for Use in a Lower Body Negative Pressure Box to  
Counteract the Effects of Weightlessness

By

Christine M. Dailey

B.S., Embry-Riddle Aeronautical University, 2011

A thesis submitted to the Department of Mechanical Engineering

College of Engineering

Embry-Riddle Aeronautical University

In partial fulfillment of the requirements for the degree of

Master of Science in Mechanical Engineering

2013

© 2013 Christine M Dailey

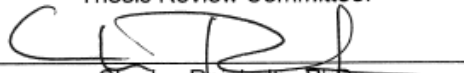
**A Novel Resistance Exercise Machine for Use in a Lower Body  
Negative Pressure Box to Counteract the Effects of Weightlessness**

by

Christine M. Dailey

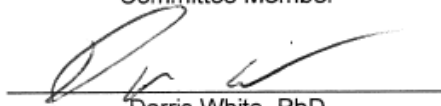
This thesis was prepared under the direction of the candidate's Thesis Committee Chair, Dr. Charles Reinholtz and Thesis Committee Members Dr. Eduardo Divo and Dr. Patrick Currier. It was submitted to the Department of Mechanical Engineering in partial fulfillment of the requirements for the degree of Master of Science in Mechanical Engineering.


Thesis Review Committee:


  
Charles Reinholtz, PhD  
Committee Chair

  
Patrick Currier, PhD  
Committee Member

  
Eduardo Divo, PhD  
Committee Member

  
Darris White, PhD  
Graduate Program Chair,  
Mechanical Engineering

  
Maj Mirmirani, PhD  
Dean, College of Engineering

  
Robert Oxley, Ph.D.  
Associate Vice President of Academics

5-3-2013

## **Acknowledgements**

This study was conducted under the partnership of Embry-Riddle Aeronautical University, USA and Pontifícia Universidade do Rio Grande do Sul, Brazil and was supported by Fund for the Improvement of Postsecondary Education (FIPSE)

# **Abstract**

Christine Marie Dailey

Physiological deconditioning is a critical problem in space, especially during long-term missions. Resistance exercise coupled with lower body negative pressure (LBNP) has been shown to be effective in counteracting some of the deconditioning related problems. This thesis describes the development of a compact and effective resistance exercise machine that works within an existing environmentally controlled LBNP Box and is designed to simulate both exercise and sitting, to prevent microgravity-induced deconditioning by simulating physiological and biomechanical features of upright exercise and daily activities. Theoretical calculations are carried out to determine whether kinematics, musculoskeletal loadings, and metabolic rate during supine exercise within the existing LBNP Box are similar to those of an upright posture in Earth gravity (1G). Preliminary results show subjects that use the resistance machine presented in this thesis will be able to elicit loads comparable to exercise on Earth, since the ground reaction forces (GRF) are greater than their body weight (BW). The largest single-leg forces during resistance exercise are 1.16 BW (232lbs) during supine position when  $\gamma$ , the angle between the horizontal and the ground pivot on the right side of the mechanism, equals 187 degrees and minimal at 0.68 BW (136lbs) when  $\gamma$  equals 177 degrees. At the lowest setting of the machine, peak resistance of the foot pedal during the

outward stroke is 196 lbf. This force, added to the force due to the 50 mmHg of negative differential pressure, gives a total force of 400 lbf, which is 2 BW.

The results suggest that this machine can be used to collect and establish a database under both terrestrial conditions and microgravity environments such as the International Space Station to enhance medical researchers' understanding of how LBNP paired with exercise impacts osteoporosis, orthostatic intolerance and cardiovascular health. The combination might also be used to enhance rehabilitation protocols.

## Table of Contents

Acknowledgements .....	4
Abstract.....	5
Chapter 1 .....	1
Introduction .....	1
Method.....	5
Four-bar linkage in conjunction with coil spring and damper system .....	6
A two member chair serves as daily activity.....	10
Mechanical Results.....	11
The integration of the multi-platform device and the existing LBNP Box.....	12
The integration of the multi-platform device and the upright device .....	13
Theoretical Results and Discussion .....	14
Summaries and Conclusion .....	18
CHAPTER II .....	20
RECOMMENDATIONS FOR FUTURE RESEARCH.....	20
INTRODUCTION .....	20
Military Relevance .....	21
Technology and Development .....	23
Concept for space flight version.....	24
Technical Comparison to Existing Exercise paired with Lower Body Negative Pressure .....	25
Chapter III .....	27



Appendixes .....	27
Introduction .....	27
Results.....	<b>Error! Bookmark not defined.</b>
Preliminary kinematic problems and solutions .....	53
References.....	55

## List of Figures

1. Human strength curve for an outward stroke of a leg-press exercise.....	4
2. Exercise equipment paired with an existing LBNP Box. Right.....	5
3. 2-D sketch.....	6
4. Prototype 1.....	6
5. Kinematic diagram.....	8
6. Projection of the kinematic diagram onto the second prototype. ....	8
7. Multi-platform's starting and end positions .....	8
8. Shows the spring-loaded knob and pin detent system .....	11
9. Second prototype .....	13
10. Final integration of the multi-platform to the existing LBNP Box.....	13
11. Final integration of the multi-platform and the upright device. ....	14
12. Static resistance curve on the outward stroke .....	15
13. The first assumed profile .....	16
14. The second assumed motion profile.....	16
15. Raw data from the electrogoniometer in the supine position.....	17
16. Variation in the user's force through a change in dimension $L_o$ . ....	17

17. Levels of blood pressure in mmHg in regards to the location within body in the specified environment. ....	21
18. Soldier using standard exercise equipment during a rehabilitation protocol.....	22
19. Exercise machines currently on the ISS.....	23
20. GRF found at a walk (left) and run (right).....	24
21. Sketch representing a treadmill, paired with lower body negative pressure.....	25
22. A treadmill paired with lower body positive pressure.....	26
23. Resistance curve calculations, implementing the spring properties. ....	39
24. Resistance curve results.. ....	39
25. Virtual work calculations.....	40
26. Moments of inertia (MOI) calculations assuming the foot pedal is negligible. ....	40
27. MOI solution for the ramp up, ramp down velocity profile.....	41
28. GRF found using a zero spring preload at $L_0$ equal to two inches assuming ramp up, ramp down velocity profile.....	41
29. MOI solution for the ramp up, ramp down velocity profile. Calculates the GRF using zero, 200 lb and 400 lb spring preload at $L_0$ equal to 0.38 inches and 1.38 inches with 50 mmHg applied. ....	42
30. GRF found using a 400 lbs spring preload at $L_0$ equal to 0.38 inches assuming ramp up, ramp down velocity profile.....	42

31. MOI solution for the ramp up, ramp down velocity profile. Calculates the GRF using 200lb and 400lb spring preload at Lo equal to 0.38 inches and 1.38 inches with 50 mmHg applied.....	43
32. MOI solution for the ramp up, constant, ramp down velocity profile. Calculations for the GRF using 200 lb and 400 lb spring preload at Lo equal to 0.38 inches. ....	43
33. GRF found using a zero spring preload at Lo equal to two inches assuming ramp up, constant, ramp down velocity profile. ....	44
34. MOI solution for the ramp up, constant, ramp down velocity profile. Calculates the GRF using zero, 200 lb and 400 lb spring preload at Lo equal to 0.38 inches, 1.38 inches and 2 inches with 50 mmHg applied.....	45
35. GRF found using a zero spring preload at Lo equal to 0.38 inches (shown in blue), 1.38 inches (shown in red), 2.0 inches (shown in purple) assuming ramp up, constant, ramp down velocity profile.....	45
36. MOI solution for the ramp up, constant, ramp down velocity profile. Calculates the GRF using zero, 200 lb and 400 lb spring preload at Lo equal to 0.38 inches and 1.38 inches with 50 mmHg applied. ....	46
37. GRF found using a 0 lb, 200 lb, and 400 lb spring preload at Lo equal to 0.38 inches, and 1.38 inches assuming ramp up, constant, ramp down velocity profile with 50 mmHg applied.....	47
38. Recorded heart rate levels for 4 subjects using the initial protocol at preliminary stages of testing. ....	48
39. Borg's scale results. ....	48

40. Recorded electromyography results.....	49
41. Muscle activity shown in the upright (left) versus supine (right) position. ....	50
42. Pressure distribution Insole .....	51
43. Subject being fitted for the pressure distribution insole .....	52
44. Subject testing the insole. ....	52
45. 3-D CAD model displays three rotational joints linearly aligned. ....	53
46. Second prototype mated to the existing trolley.....	54

# Chapter 1

## Introduction

Gravity has had an integral effect on the development of life on Earth over millions of years and has shaped the anatomy and physiology of human beings. Exposure to microgravity has been shown to affect the body, causing it undergo a reduction in heart size and blood volume, impaired balance control, changes in nervous system sensitivity, decreases in bone and muscle mass, and reduction of the immune function. Astronauts in space during short or long-term missions have demonstrated these physiological changes, known as space deconditioning, which may lead to undesirable health consequences and to operational difficulties, especially during emergency situations.

With the recent advent of space tourism and with longer space missions planned, greater numbers of astronauts will work and live in low-gravity environments, and the need to understand the in-flight and post-flight consequences of this will become more significant. The physiological adaptations are less problematic in space, but are more pronounced after a return to Earth. The mechanical unloading affects the musculoskeletal system even in short-duration space flights. It has been reported that after only 2 weeks in space, muscle mass can decrease by 20%. For missions of 3-6 months this can rise to 30%, especially affecting postural muscles [7]. The decrease in bone mass is also of great concern to space physiologists and physicians, as the normal processes of bone

formation and resorption are disturbed, favoring a loss of bone tissue [2]. This process begins almost immediately upon introduction into microgravity, and can range between 1% and 2% of bone mass loss per month [6]. One of the first responses to space flight is the shift of blood and body fluids towards the upper body, with subsequent adaptations occurring over a few days to lower overall blood volume through activation of several mechanisms [3]. It is upon return to Earth that the cardiovascular deconditioning raises concerns by producing significant orthostatic intolerance and decreasing aerobic performance [5].

Many different types of countermeasures have been developed, ranging from specific diets to heavy exercise protocols that must be performed daily by the astronauts during a space mission. Ideally, the best way to counteract consequences of space deconditioning would be the use of artificial gravity through centrifugation or other biomechanical stressors for periods of time during microgravity exposure.

Among the countermeasures currently under testing, daily exercise in space seems to be the most complete, because it prevents bone demineralization, muscle loss and cardiovascular deconditioning. The effectiveness of exercise protocols and equipment for astronauts in space, however, are unresolved and still under discussion. Studies indicate that all exercise in space to date has lacked sufficient mechanical and physiological loads to maintain preflight musculoskeletal mass, strength, and aerobic capacity [4, 9, 16, 17]. Recently, researchers have been pairing exercise with LBNP. The LBNP Box is a sealed chamber into which the human subject is partially inserted. A seal near the waist allows a vacuum to be applied to the chamber, thus creating a lower relative pressure on the subject's lower body. This lower pressure helps pull bodily fluids

toward the feet.

Combining the resistive force from exercise and a uniformed pressure distribution to the lower extremities has shown to be an efficient solution for counteracting microgravity-induced deconditioning during terrestrial testing. The most recent study of the addition of a treadmill to an LBNP Box has demonstrated that it is able to simulate physiological and biomechanical features of upright exercise [22]. However, its mechanical design lacks mobility and is both large and heavy, making it unsuitable for space flight.

The research presented in this thesis offers as an alternative to the treadmill. The purpose was to design a lightweight, compactable exercise machine combined with a collapsible chair that could be easily integrated into a smaller, existing LBNP Box. The machine is to offer a constant load path to maintain compressive loads on the musculoskeletal system and aid to the human body as much as possible. The human body is a highly nonlinear mechanical device from the standpoint of generating forces over a given cycle of motion. The exercise known as a leg press is a good example of this. Figure 1 shows the human strength curve for the leg-press exercise. This is a plot of the maximum force a user can produce at each point in the outward cycle of a leg press. Not surprisingly, we are able to generate far more force at the extreme position (when the knee joint is at full extension) than when the knee is sharply bent.



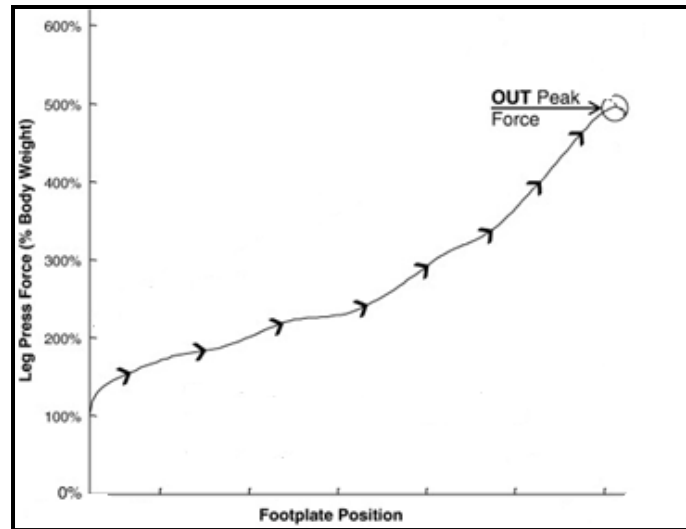


Figure 1. Shows the human strength curve for an outward stroke of a leg-press exercise; force in magnitude versus degree in stroke. Additional information of this graph is provided in reference [19].

Mechanical work and physiology stress in the muscles will be nearly optimized when the resistance provided by a machine most nearly matches this strength curve [22]. The resistance curve should match the human strength curve for optimal efficiency in strengthening muscle and stressing bone. Although the strength curve varies from user to user, the general shape of the curve is approximately maintained.

Our goal in designing the alternative system was to match the resistance provided by the machine with the human strength curve in a leg press exercise. This requires an adjustable level of resistance that will lead to a vertical shift in magnitude of resistance while keeping the general shape of the curve to accommodate each user. In this thesis, the alternative machine is referred to as a multi-platform. The multi-platform is to be a compact system that offers a constant load path throughout the cycle, and is to conform to the most natural movement of the human body as possible. The design was driven by both the dimensions of an existing LBNP Box and by the average size astronaut.

Averaging the size and weight of astronauts allowed for an initial range of resistance the multi-platform would impose on the user to simulate forces equal to one or more of their BW.

## Method

A 3-D SolidWorks model of the multi-platform is shown in Figure 2 (*right*). The integrated system, the multi-platform and the existing LBNP Box, is shown in Figure 2 (*left*) where the brown-colored links simulate human legs and feet. The green and red tubes represent cooling ducts that provide an environmentally controlled atmosphere. The system will stress the lower extremities of the human body by providing both a resistance force due to the exercise machine and a pressure force caused by the LBNP Box. In combination, these forces counteract the deleterious effects of microgravity-induced syndrome.

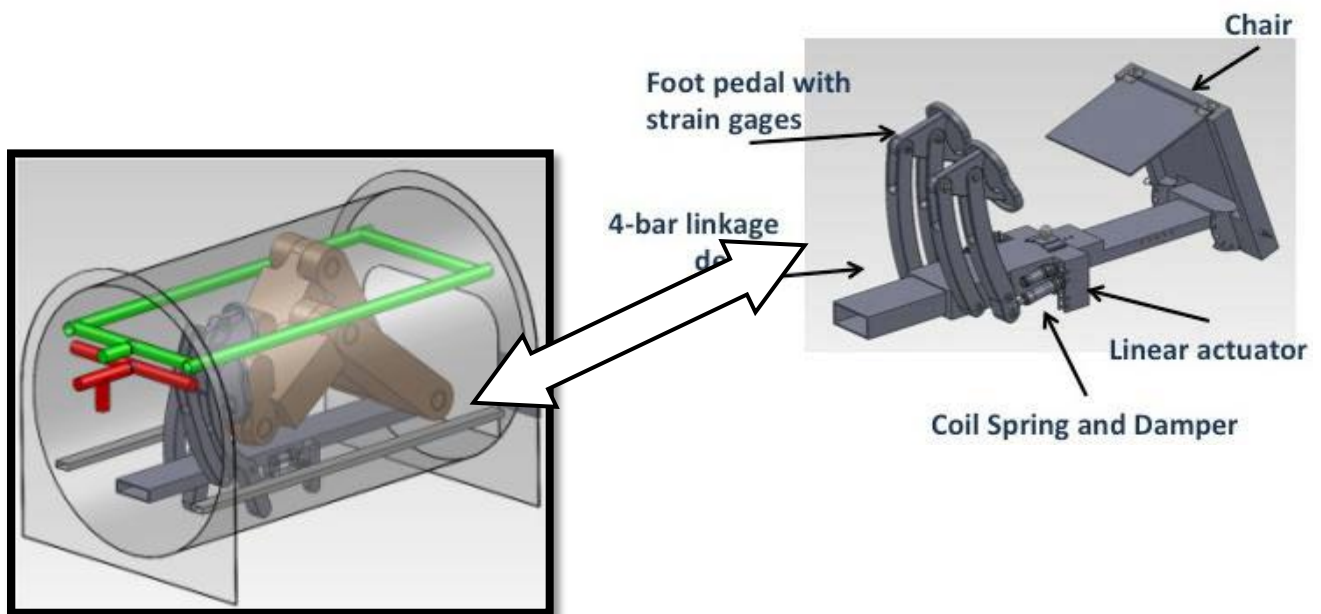


Figure 2. left, displays the Exercise equipment paired with an existing environmentally controlled LBNP Box. Right, displays a 3-D CAD model of the multi-platform device.

# Four-bar linkage in conjunction with coil spring and damper system

## *Kinematics*

Classic techniques in kinematics were used to design and optimize the geometry and resistance which would produce desirable motion and force properties. As shown in Figure 3, if a force is applied by the user to the foot pedal, the parallelogram linkage will guide the foot pedal along a circular-arc path at a fixed angle relative to the frame of the machine. This is important for maintaining a generally perpendicular relationship between the lower leg and the foot. Applying forces in this manner to the musculoskeletal system is believed to be one of the most efficient ways to counteract osteoporosis [20].

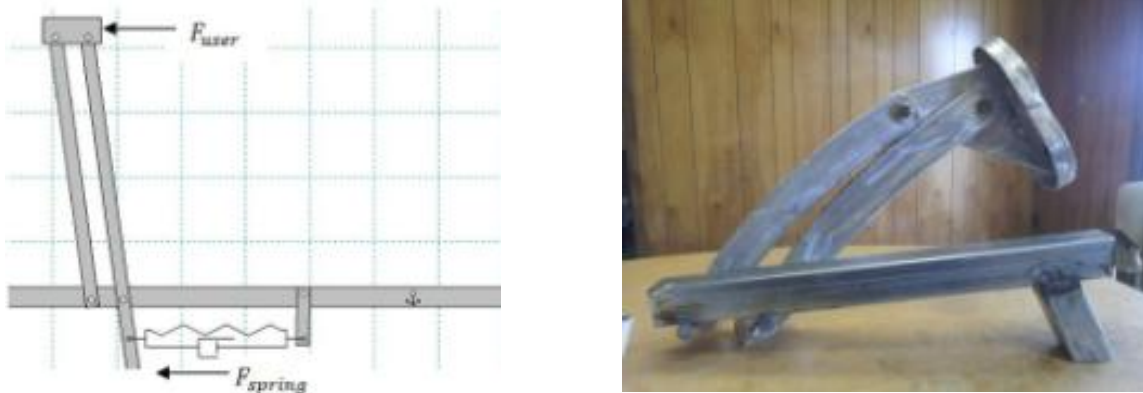


Figure 3. (left), 2-D sketch of a four-bar parallelogram paired with a sliding crank mechanism. The sliding crank is a spring and damping system that offers a variable resistance. Figure 4. (right), A photograph of the first prototype which was TIG welded out of sheet aluminum alloy and served as a rapid mock-up of the 3-D CAD model shown in Figure 2 to ensure the idea was practical.

Referring to Figure 5, loop closure, Equation 1, and velocity loop, Equation 2, will

yield the position,  $s$ , and velocity,  $\dot{s}$  of the slider crank mechanism given the input position,  $\theta$ , and velocity,  $\dot{\theta}$ . Static resistance is dependent only on the value of  $\theta$ , which determines the compression of the spring, and the geometry of the device.

Dynamic resistance depends on the user's motion profile ( $\dot{\theta}$ ).

$$l_o \hat{j} - l_1 - l_2 e^{j\theta} - s e^{j\gamma} = 0 \quad (1)$$

$$\hat{j} l_2 \dot{\theta} e^{j\theta} - \dot{s} e^{j\gamma} - \hat{j} s \dot{\gamma} e^{j\gamma} = 0 \quad (2)$$

Two different motion profiles were used to calculate the inertia and damping force. The first profile had constant angular acceleration of the foot pedal link to start and end the motion cycle and a period of constant velocity in between. The second motion profile was similar, but with no constant velocity motion period separating the periods of positive and negative constant acceleration. An electrogoniometer was used as a method in confirming which assumed motion profile was most accurate. The meter was applied to the subject's left knee, centered directly over the rotational joint.

Once the position and velocity loop equations have been solved, virtual work can be used to find the resistive force,  $F_{user}$ , as a function of position,  $\theta$ , from Equation 3.

$$I^* \ddot{\theta} \dot{\theta} + F_{user} \dot{\theta} l_3 + F_{spring} \dot{s} = 0 \quad (3)$$

The inertial term in Equation 3,  $I^* \ddot{\theta} \dot{\theta}$ , is based on a position-dependent equivalent inertia approach described in reference Suh and Radcliffe [21]. Note that the motion of the user is expected to be slow, so dynamic effects, including the force of the damper, are expected to be small. The damper is incorporated to prevent rapid movement in the event that the user's foot slips off the pedal. It also helps to discourage high-speed exercise motion.

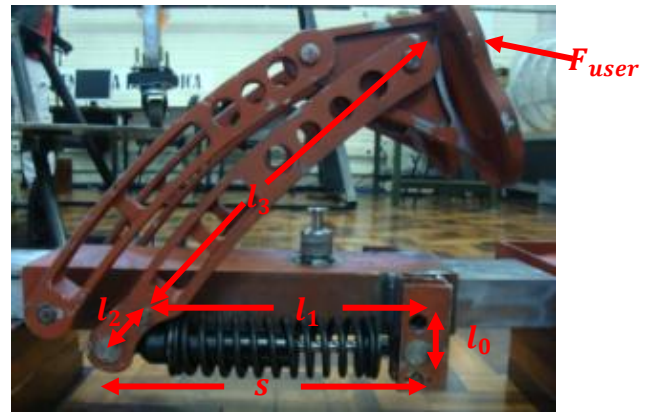
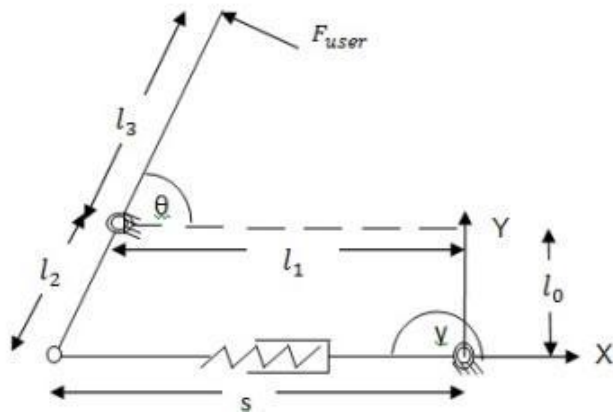


Figure 5. (left), Kinematic diagram of the mechanism in which Equations 1 and 2 are based. Figure 6. (right), Displays the projection of the kinematic diagram, shown in Figure 5, onto the second prototype.

**Resistance**

A coil spring and damper system, acting as the prismatic joint in a slider-crank mechanism, provides resistance. Using this force-generating slider-crank system in conjunction with the 4-bar linkage creates a nearly optimal resistance curve that approximates the strength curve of the user through the range of motion, shown in Figure 7 [15].

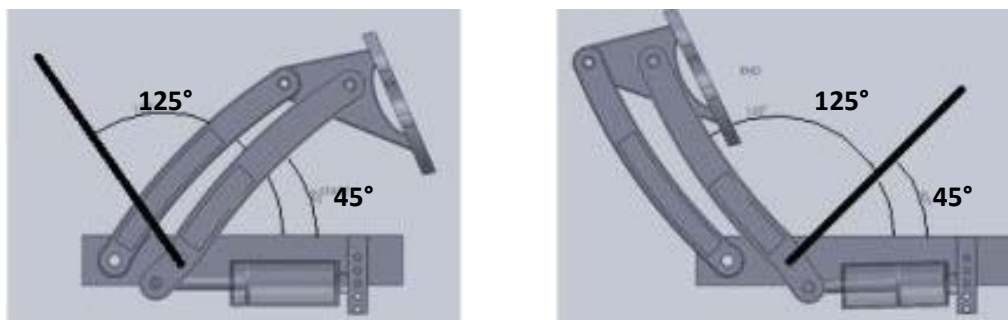


Figure 7. (left), Multi-platform’s starting position with the spring at a resting position. (Right), Multi-platform’s end position with the spring fully compressed.

This system creates the high forces and stresses needed to maintain bone density, and

optimize the cardiovascular workout. The slider-crank mechanism compresses the linear spring, creating an increasing resistance throughout the movement and causing the largest load to be applied when the user's leg is fully extended and in turn provides the desired optimized profile in relation to the human strength curve.

### ***Resistance due to inertial forces***

The user must overcome the static spring forces, the damping forces, and the inertia forces generated by acceleration of the links of the exercise device. Inertia forces are incorporated in Equation 3 by calculating an equivalent inertia of the system,  $I^*$ , that varies with position. Equation 4 from reference Suh and Radcliffe shows how such an equivalent inertia is found.

$$\frac{1}{2}I^* = \sum_{i=1}^n \frac{1}{2}m_i(\dot{x}_i^2 + \dot{y}_i^2) + \frac{1}{2}I_i\dot{\theta}_i^2 \quad (4)$$

Equation 4 takes into account the mass ( $m$ ) and inertia ( $I$ ) of every moving link in the mechanism. While all links contribute to the total user force, the mass of the foot pedal is of special concern. Because the foot pedal is at the extreme end of link 3, it has the largest peak velocities and accelerations. It is also the most massive element in the prototype system. One goal in designing the device is to minimize inertial forces. This allows us to shape the static resistance curve through kinematics to be as similar to the human strength curve as possible. Dynamic forces will change the shape of this curve as a function of how rapidly the user moves the foot pedal. Further analysis will show that the dynamic forces can be kept small.

### ***Biomechanics***

GRF are created by static and dynamic loading. The forces experienced in 1G are due to the user's weight (static) and the dynamic loading due to movement. To simulate

forces equivalent to those experienced in 1G, the GRF must be equal to or greater than 1 BW. As shown in Equation 5, the GRF are directly related to the pressure differential force and the total user force applied by the user to move the foot pedal. Note that the vacuum feature of the LBNP Box will not be used during preliminary testing.

$$\text{GRF} = (\text{Pressure Differential Force}) + (\text{Total User Force}) \quad (5)$$

Equation 5 states that GRF found during exercise in LBNP while supine and in microgravity equals the pressure differential force plus the total user's force. The pressure differential force equals the product of the body cross-sectional area ( $A_{xy}$ ) and the pressure differential ( $\Delta P$ ) across the LBNP Box, which will be assumed to equal 50 mmHg. The total user's force includes the inertial forces caused by the geometry of the exercise portion of the multi-platform and the force required to overcome the resistance of the coil spring and damper system.

## **A two member chair serves as daily activity**

The posterior side of the lower extremities are accustomed to 2/3 BW between six and eight hours a day. The chair simulates this daily activity of sitting by translating a fixed linear force to the active areas. The force applied will be simulated from the negative pressure in the LBNP Box.

As shown in Equation 6, if the subject is motionless, the Total User Force term in equation 5 equals zero.

$$\text{GRF} = A_{xy} * \Delta P \quad (6)$$

The chair is adjustable in both angle and linear distance via use of quick release pins and a sliding member. It is easily foldable and has a resting position horizontal to the center bar. The chair is cushioned by foam and covered with leather allowing the user to

both exercise and sit comfortably. Due to time constraints the chair will not be included in the protocol for this study.

## Mechanical Results

The multi-platform device was designed to accommodate the average sized astronaut, to be integrated within an existing LBNP Box, and to simulate responses found in both upright exercise and the daily activity of sitting. To collect comparable data the multi-platform had to go from a horizontal position within the LBNP Box to vertical position outside the LBNP Box and allow subjects to perform the same protocol.

To accommodate a wide range of users, aside from the average astronaut, the location of the pedal system is adjustable relative to the seat location. This is accomplished through the use of a sliding member that allows the user to adjust the position of the device along a rectangular base frame. The sliding member is easily adjusted over a 14 cm range by a spring-loaded knob and pin detent system shown in Figure 8.

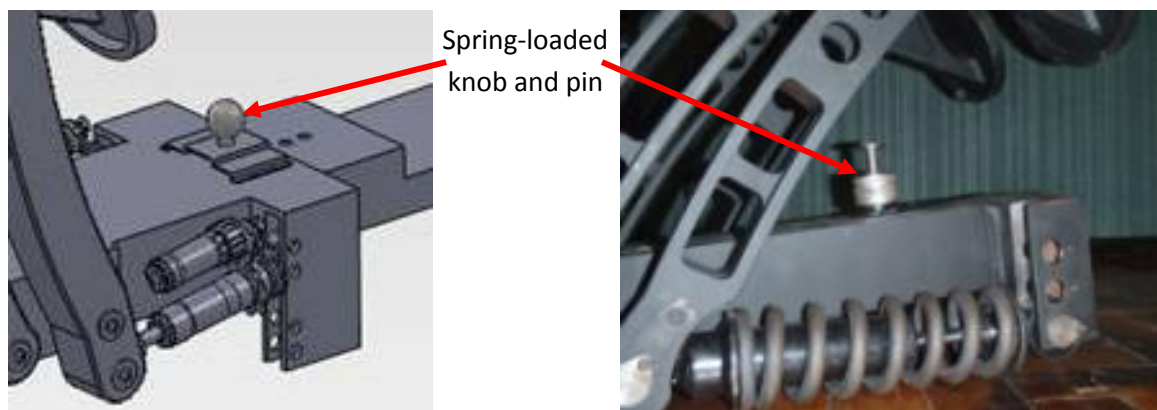


Figure 8. Shows the spring-loaded knob and pin detent system. The photograph on the right is the third prototype.

To further accommodate users of different strengths, an additional adjustment has



been designed into the machine. This feature personalizes the device by changing the initial preload in the spring. The geometry of the slider-crank mechanism is changed by lowering the ground pivot on the right side of the mechanism, as shown in Figure 5 and 6. Lowering this pivot (changing the value of  $L_0$ ) generally causes a vertical shift in the resistance curve.

In the next design iteration, a linear actuator will be incorporated to control the position of the above-mentioned ground pivot. The adjustment will occur automatically based on the user's heart rate. The user will be required to keep a steady target HR that will be determined using Equation 7 and monitored throughout the workout.

$$HR_{target} = ((HR_{max} - HR_{rest}) * \%_{intensity}) + HR_{rest} \quad (7)$$

In this study, the spring was changed manually with the use of quick release pins.

## **The integration of the multi-platform device and the existing LBNP Box**

The multi-platform device is manufactured to be removable, without disassembly, from the LBNP Box inner structure. It attaches to the trolley system, shown in Figures 9 and 10, making it maneuverable and easily accessible, which allows the user to adjust it to their personal settings outside of the LBNP Box. The parallel arms and seat collapse horizontally to the center bar, allowing the removal process to be quick, easy, and safe.

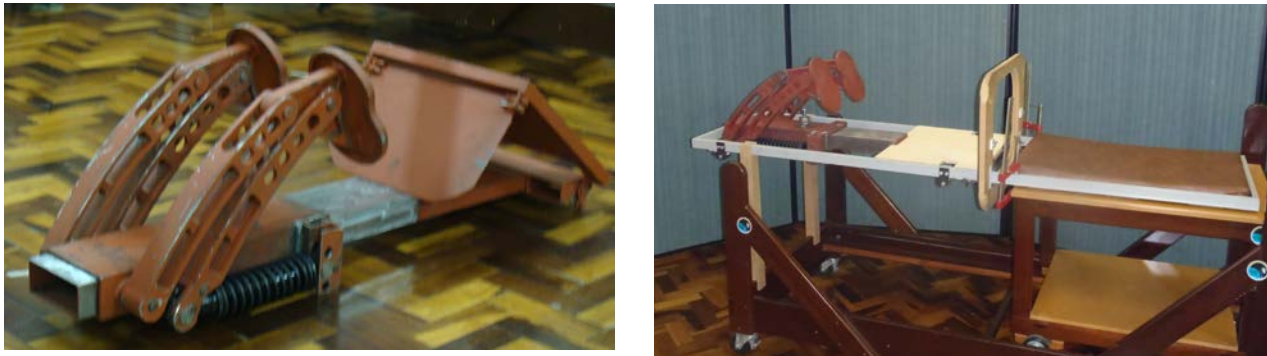


Figure 9. The left photo shows the second prototype with the chair in its upright position. The right photograph shows the second prototype (chair down) attached to the trolley which is inserted into the LBNP Box.



Figure 10. The left photo shows final integration of the multi-platform to the existing LBNP Box. The right photo displays a close up of the multi-platform outside of the LBNP Box.

## **The integration of the multi-platform device and the upright device**

The physiological and biomechanical responses of each subject will be recorded in the supine and upright position in order to collect comparative data. In the upright position, there will be no added negative pressure or suction force, only the effects of gravity. Data collected in upright position will be compared to data taken in the supine position. If the

LBNP is effective than the user forces, heart rate and expended energy should be comparable and similar between the two configurations.

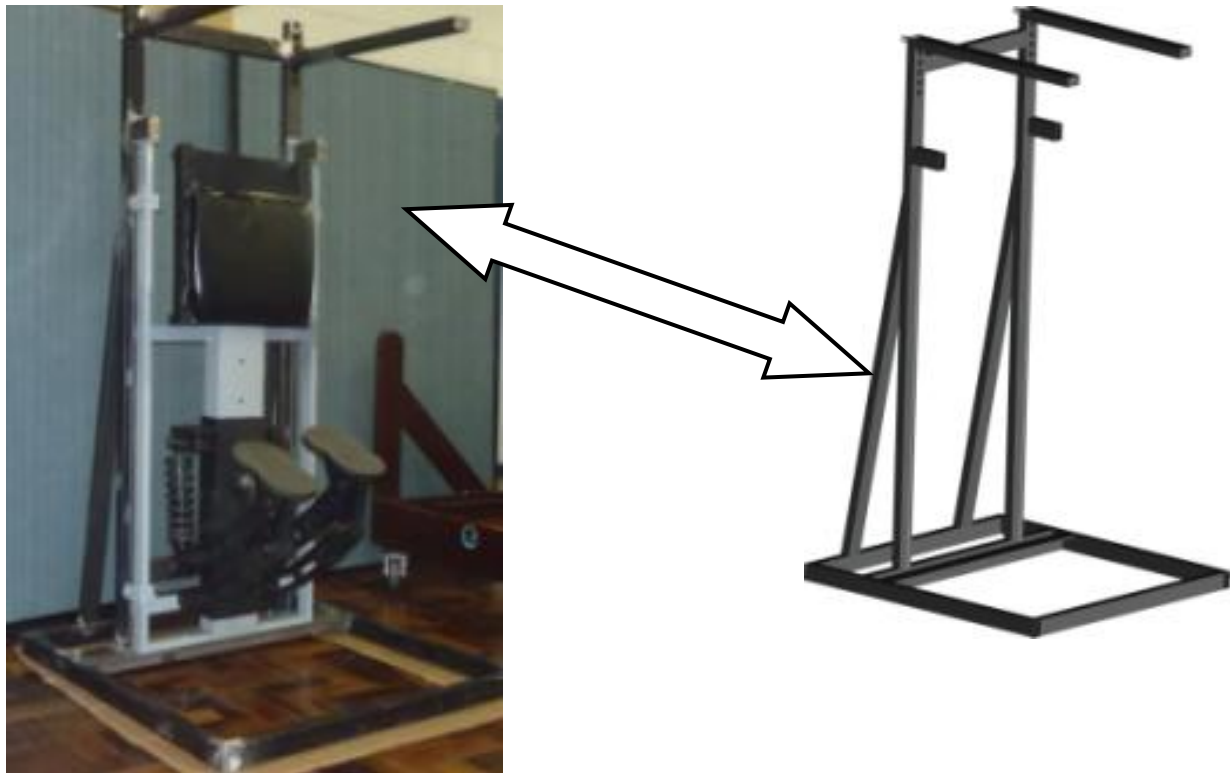


Figure 11. A 3-D CAD model, *right*, of the upright device that will support the multi-platform in a vertical position. The *left* photograph is the final integration of the multi-platform and the upright device.

## Theoretical Results and Discussion

The multi-platform device was to approximate the resistance provided by the machine with the human strength curve in a leg press exercise shown in Figure 1. As shown in Figure 12, the slider-crank mechanism used in the multi-platform creates an excellent approximation to the human strength curve when considering only the resistance of the spring. By limiting dynamic forces, the results show that the overall machine exhibits an excellent resistance curve under typical operating conditions.

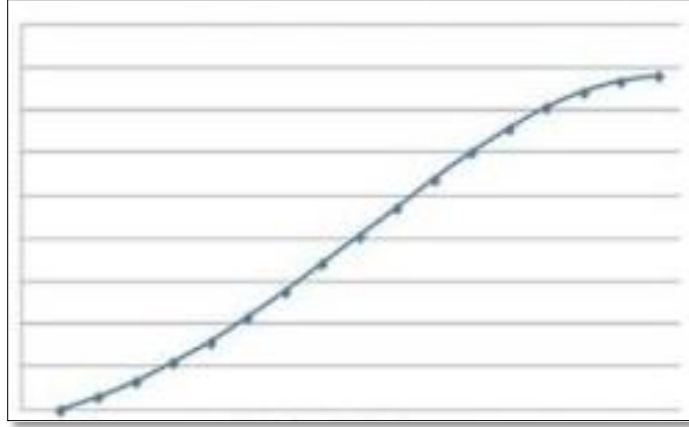


Figure 12. Static resistance curve on the outward stroke for the multi-platform considering only spring resistance.

The theoretical resistance provided by the multi-platform device has been calculated under a set of assumed conditions. This analysis uses the actual link masses and inertias from the prototype with the exception of the foot pedal link. In the next iteration, these values should be reduced. This should result in improved resistance profiles. The most important assumption necessary to perform a complete analysis is the user's motion profile. Since the foot pedals reciprocate, we know that their angular velocity will be zero at the beginning and end of each stroke. Velocity should ramp up to a peak somewhere between these endpoints. But, there is no way to precisely predict how the user will accelerate and decelerate. We do know from testing that a typical user moves at about one cycle of motion per second. The results from the two assumed motion profiles are shown in Figures 13 and 14. In both figures, the red curve shows the user force on the foot pedal due to the resistance of the spring, the green curve shows the user force on the pedal due to dynamic effects, and the blue curve is the net user force on the pedal through a 0.5 second stroke.

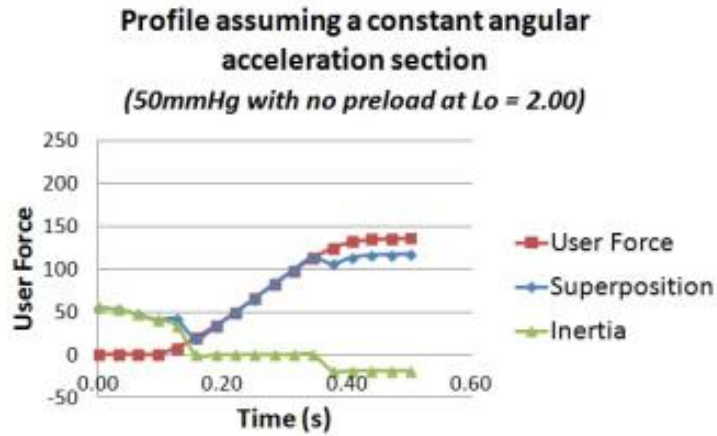


Figure 13. The first assumed profile shows a constant angular acceleration to start and end the motion cycle and a period of constant velocity in between.

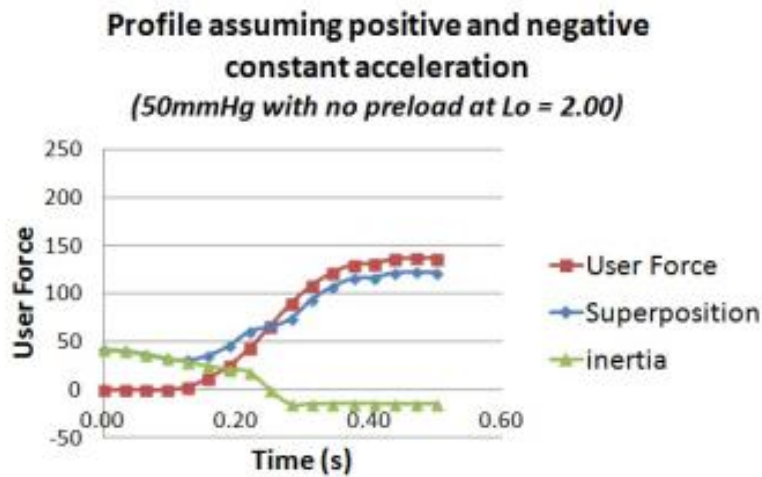


Figure 14. The second assumed motion profile shows positive and negative constant acceleration without a period of constant velocity.

The output data shown in Figure 15, from the electrogoniometer indicated that the user is generally accelerating or decelerating the foot pedal, with little or no constant velocity in the middle. As a result the second velocity profile will be assumed for all subsequent analysis.

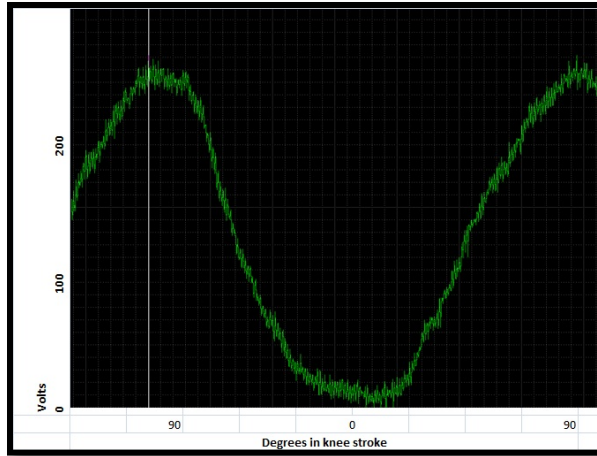


Figure 15. Raw data from the electrogoniometer in the supine position.

The analysis also considered the effect of varying the spring preload and the effect of the LBNP Box pressure difference on the foot pedal forces exerted by the user. The graphs in Figure 16 show the variation in user foot pedal force as the spring preload increases through a change in the adjustable dimension  $L_0$ .

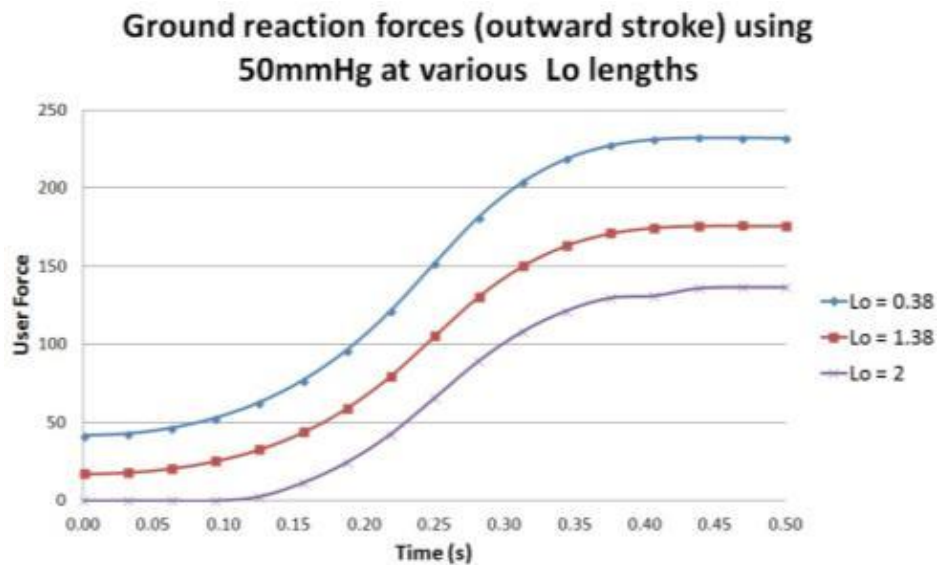


Figure 16. Variation in the user's force as the spring preload increases through a change in dimension  $L_0$ .

## Summaries and Conclusion

The compact, easily transportable, multi-platform device is designed to simulate both exercise and the daily activity of sitting. The exercise portion of the device creates stress on the lower extremities by supplying a variable resistance to a reciprocating foot pedal. This resistance is created from a coil spring and damper system acting through a 4-bar linkage. The resisting force increases as a function of leg extension to maximize work done by the user in each cycle of motion. The sitting portion of the multi-platform device creates a resistance applied to the posterior side of the lower extremities by the use of a chair. The chair is adjustable in angle to fit each subject and to simulate a force  $2/3$  BW, mimicking the posterior forces equivalent to the human activity of sitting between six and eight hours a day.

The multi-platform is paired with an existing LBNP Box to add an evenly distributed pressure-induced stress to the lower extremities. However, the LBNP Box constrains the length of the subject's lower extremities, waist to sole of foot, to range from 70cm to 82cm. By combining resistance exercise and lower body negative pressure, the subject will experience one or more times BW in stress on their musculoskeletal, cardiovascular and nervous systems. By achieving 1 BW or greater (artificial gravity) during exercise and  $2/3$  BW during sitting, the gap between the precondition and post condition syndrome will become smaller. The largest single-leg forces during resistance exercise are 1.16 BW (232lbs) during supine position when  $\gamma$ , the angle between the horizontal and the ground pivot on the right side of the mechanism, equals 187 degrees and minimal at 0.68 BW (136lbs) when  $\gamma$  equals 177 degrees. We conclude that the exercise portion of the multi-platform was able to elicit loads comparable to exercise on

Earth since the forces were greater than 1 BW and predict that when paired with LBNP the maximum resistance load can be as low as 196 lbf when the LBNP is set for the recommended 50 mmHg to achieve, at maximum, 2 BW.

Future versions of the machine should have lighter links and hence improved overall resistance curves. The multi-platform is fabricated from steel, which causes the inertia forces in the above calculations to be larger than desired. The angle of the foot pedal needs to be adjusted so that the user's foot maintains an angle closer to 90° throughout the entire cycle rather than just toward the beginning and the end of the stroke. Currently, too much of the force from the subject's foot is directed along the link, resulting in user forces that are somewhat higher than desired for the first half of the pedal stroke. Another future improvement includes a linear actuator to change the level of resistance based directly off the subject's heart rate.

Overall, the combination of the multi-platform and the LBNP Box show great promise for minimizing deconditioning and for providing a safe, compact, lightweight and efficient way for space travelers to exercise.



## **CHAPTER II**

### **RECOMMENDATIONS FOR FUTURE RESEARCH**

#### **INTRODUCTION**

Recommendations for this research is to collect and establish a database under the International Space Station (ISS) to enhance medical researchers understanding of how lower body negative pressure (LBNP) paired with exercise impacts osteoporosis, orthostatic intolerance and cardiovascular health in order to assist both war veterans' and astronauts by offering a more effective rehabilitation protocols and providing a method to ensure safety while performing duties.

Each subject will have their cardiovascular responses and biomechanical measurements taken continuously throughout the exercise protocol.

An electronic monitoring system will track the astronaut's cardiovascular responses to avoid over-exertion. Sensors in the multi-platform elements will measure the ground reaction force (GRF) and provide visual feedback to the user to ensure correct form is used.

Data collection in a microgravity environment will yield faster results then terrestrial testing alone. This is due to the acceleration of bone loss, muscle atrophy, and poor cardiovascular health experienced in microgravity. Bone loss, muscle atrophy, and poor

cardiovascular health are developed for different reasons among astronauts versus injured soldiers/veterans; however the rehabilitation necessary for recovery appears to be very similar [24, 25, 26].

## Military Relevance

The human body undergoes several physiological changes in low gravity at an accelerated rate, including reduction in heart size and blood volume, impaired balance control, and decreases in bone and muscle mass as shown in Figure 17. These physiological changes lead to undesirable health consequences and to operational difficulties, especially during emergency situations.

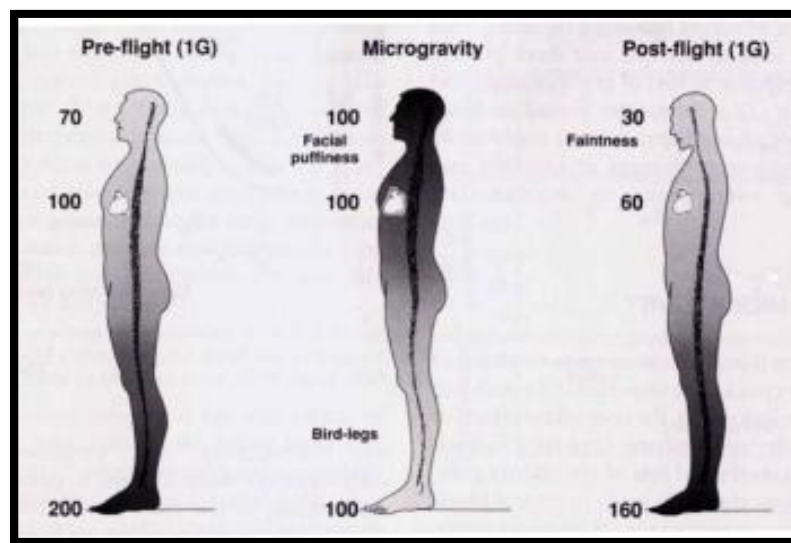


Figure 17. The numbers shown above denote the levels of blood pressure in mmHg in regards to the location within body in the specified environment [34].

It has been reported [27] that bone structure and density, after a six month mission, had not returned to normal at one year and is said to take much longer with current rehabilitation protocols.

According to the Military Times, of the more than 24.8 million veterans, 624,000, from Iraq and Afghanistan wars, have filed disability claims. According to the Budget of the U.S. Government the healthcare in FY 2012 equaled 61.85 billion dollars which in part, under Function 700: Veterans Benefits and Services, goes to rehabilitation. (A 10.6% increase over 2010 to meet increased demands) [23]. The vets spend months (and sometimes years) in rehabilitation, many at the Brooke Army Medical Center in San Antonio, TX, home to the largest inpatient medical facility in the Department of Defense [29].



Figure 18. Soldier using standard exercise equipment during a rehabilitation protocol.

Rehabilitation time is believed to be reduced by the technology of combining two forms of stress applied to the body. Each stress, when performed on its own, has shown to be insufficient at overcoming bone loss, and inefficient at overcoming muscle atrophy and poor cardiovascular and nervous systems functions. However, when performed together it is believed to successfully overcome each.

## Technology and Development

Prior studies indicate that all exercise in space to date has lacked sufficient mechanical and physiological loads to maintain preflight musculoskeletal mass, strength, and aerobic capacity. This is because the existing equipment provides one form of stress at a time.

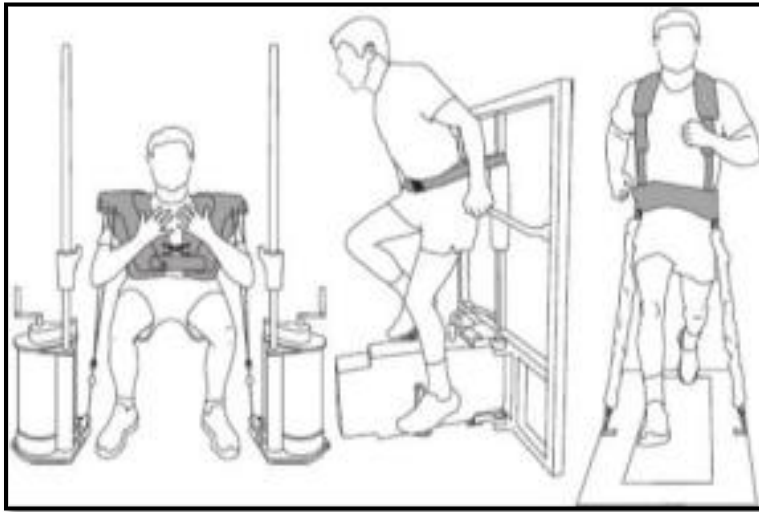


Figure 19. Resistive Exercise Device (RED), Existing equipment Cycle Ergometer with Vibration Isolation and Stabilization System (CEVIS), Treadmill Vibration Isolation System (TVIS) [33].

Bone mineral density is lost at a rate of 1.4–1.5%/month at the hip and 0.9%/month at the spine in microgravity, compared to 0.5-1%/yr in 1G. Crewmembers returning from a six month mission indicated up to a 20% reduction in muscle volume in the lower extremities [27].

In addition to exercise, electrical stimulation, load suits, pharmacologic therapy, and artificial gravity have been considered. However, only some of these methods have been implemented in space, and they have not been successful in preventing bone and muscle loss.

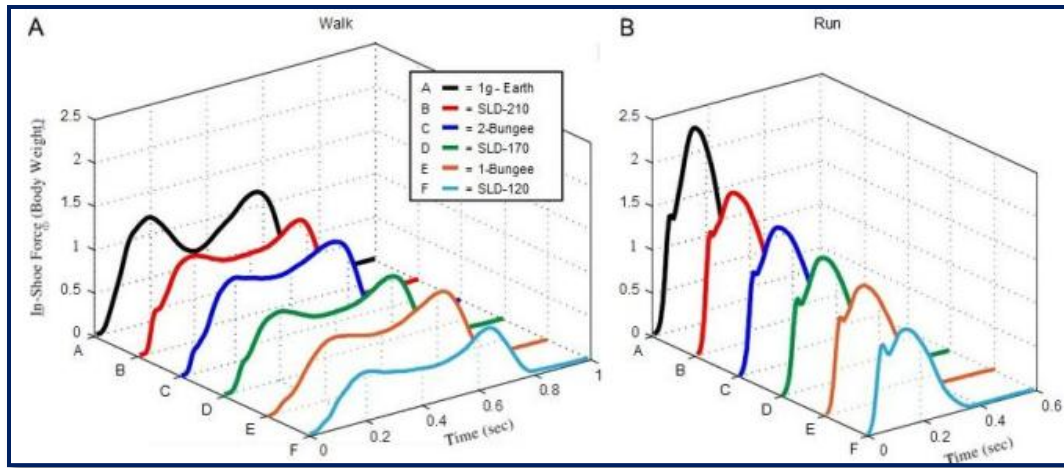


Figure 20. The graphs represent the GRF found at a walk (*left*) and run (*right*). The black line denotes the GRF found on earth while the colors denote the GRF found on the ISS using different strength bungees. These graphs state that no matter the amount of resistance added the GRF found on the ISS will not equal the GRFs found in 1G [33].

### Concept for space flight version

The novel exercise machine referred to as multi-platform will be made of mostly carbon fibers to ensure light weight and collapsibility and designed to be assembled with little or no tools at all. The LBNP Box will be transformed into an inflatable structure which can be deployed for use and stowed for space savings. A seal near the waist allows a differential pressure to be applied to the lower extremities. This acts as a suction force that pulls bodily fluid back toward the feet relieving unwanted pressure toward the upper body.

## Technical Comparison to Existing Exercise paired with Lower Body Negative Pressure

Researchers have shown, through terrestrial testing, that it is possible to decrease the gap between preflight and post flight syndrome by pairing exercise with LBNP [1], however their mechanical concepts lack, compatibility, and efficiency. The current LBNP Box is paired with a standard 450W treadmill, 193 x 127 x 128 cm, weighing in at 90kg.

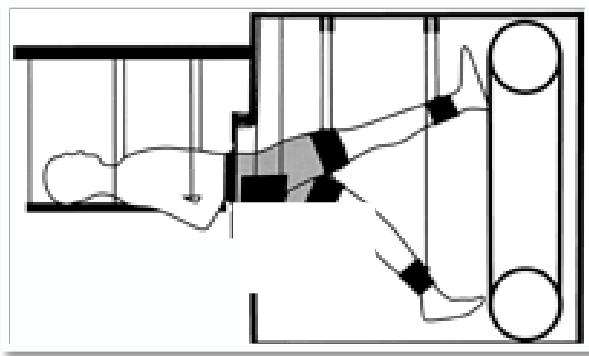


Figure 21. Sketch representing the current exercise machine, a treadmill, paired with lower body negative pressure [1].

Through antigravity machines, used in rehabilitation protocols, the first phase of bone/muscle restoration becomes easier by taking the weight off the limb [30, 31]. This quickly becomes ineffective. After the initial recovery of a fracture, the bone must experience compression forces (found in exercise) to heal properly [24]. For a bone to heal at a faster rate the compression forces need to be greater than one BW (1G).



Figure 22. A treadmill paired with lower body positive pressure [30].

This future research holds the potential to surpass current technology by

- Making the system inflatable/expandable to more than twice its stowed envelope weighing in at 5.5 kg and consuming a nominal 380 W which includes the on-board data collection and storage.
- Adding a sedentary daily activity in addition to the pure-mechanical exercise device.
- Successfully maintaining pre-flight cardiovascular and biomechanical responses which are necessary to maintain the health of each astronaut during space missions and to improve rehabilitation protocols.
- Providing a differential pressure that can be both negative and positive to accommodate each phase in the rehabilitation process.

## Chapter III

### Appendixes

#### Introduction

Using classic techniques in kinematics, the mechanism has been designed and optimized to provide an increasing resistance throughout the movement, causing the largest load to be applied when the user's leg is fully extended.

Referring to the free body diagram below, loop closure, Equation 1, and velocity loop, Equation 2, will yield the position,  $s$ , and velocity,  $\dot{s}$  of the slider crank mechanism given the input position,  $\theta$ , and velocity,  $\dot{\theta}$ . Static resistance is dependent only on the value of  $\theta$ , which determines the compression of the spring, and the geometry of the device. Dynamic resistance depends on the user's motion profile ( $\dot{\theta}$ ).

Two profiles were taken into consideration: *ramp-up/ramp-down* and *ramp-up/constant/ramp-down*. These are assumed profiles.

The following gives a step-by-step solution to the position and velocity loop equations. Then shows how virtual work is used to find the resistive force,  $F_{\text{user}}$ , as a function of position,  $\theta$ ,

Given/Assumed

The motion of the user is expected to be slow, so dynamic effects, including the force of the damper, are expected to be small. The damper is incorporated to prevent



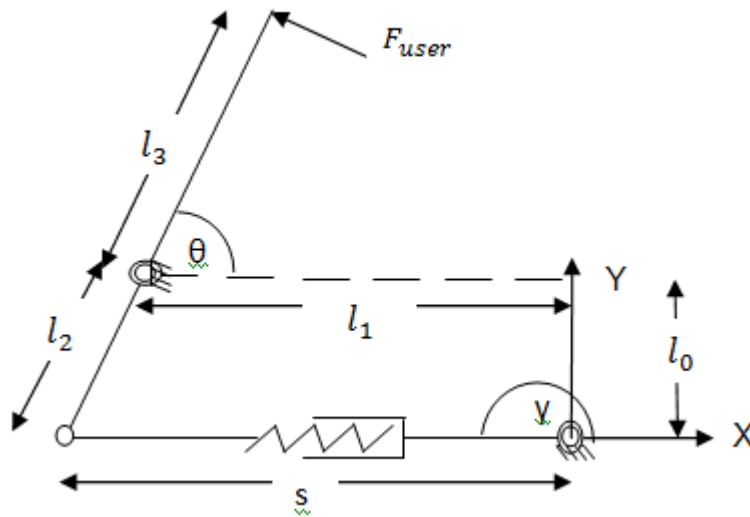
rapid movement in the event that the user's foot slips off the pedal. It also helps to discourage high-speed exercise motion. The inertial term in Equation 3,  $I^*\ddot{\theta}$ , is based on a position-dependent equivalent inertia approach described in Suh and Radcliffe.

$$l_0\hat{j} - l_1 - l_2e^{j\theta} - se^{j\gamma} = 0 \quad (1)$$

$$\hat{j}l_2\dot{\theta}e^{j\theta} - \dot{s}e^{j\gamma} - \hat{j}s\dot{\gamma}e^{j\gamma} = 0 \quad (2)$$

$$I^*\ddot{\theta} + F_{user}\dot{\theta}l_3 + F_{spring}\dot{s} = 0 \quad (3)$$

### Free Body Diagram: Kinematic diagram of the mechanism



### Method

*Loop Closure*

#### Known

$$l_0 = 1.38''$$

$$l_1 = 10.82''$$

$$l_2 = 1.95''$$

$$l_3 = 15.30''$$

$\theta = \text{user input}$

#### Unknown

$\gamma$

$s$

## Solution

Loop closure

$$l_0 \hat{j} - l_1 - l_2 e^{j\theta} - s e^{j\gamma} = 0$$

Separate into real and imaginary parts to form two equations. Two unknowns require two equations.

$$RE: l_1 - l_2 \cos(\theta) - s \cos(\gamma) = 0$$

$$IM: l_0 - l_2 \sin(\theta) - s \sin(\gamma) = 0$$

Note:  $\sin(\theta)^2 + \cos(\theta)^2 = 1$  therefore square both eq.'s and add to eliminate  $\gamma$ . We are known

$$l_1^2 + 2l_1 l_2 \cos(\theta) + l_2^2 \cos(\theta)^2 + l_0^2 + l_0 l_2 \sin(\theta) + l_2^2 \sin(\theta)^2 = s^2 \sin(\theta)^2 + s^2 \cos(\theta)^2$$

-Combine like terms

$$l_0^2 + l_1^2 + l_2^2 + 2l_2(l_1 \cos(\theta) + l_0 \sin(\theta)) = s^2$$

-Solve for s

$$s = \sqrt{l_0^2 + l_1^2 + l_2^2 + 2l_2(l_1 \cos(\theta) + l_0 \sin(\theta))}$$

s is now solved. However  $\gamma$  still remains unknown. Returning to the RE and IM equations will allow  $\gamma$  to be solved for. (eliminate s this time)

$$RE: l_1 - l_2 \cos(\theta) - s \cos(\gamma) = 0$$

$$IM: l_0 - l_2 \sin(\theta) - s \sin(\gamma) = 0$$

Note: Use division to eliminate s. Note that  $\tan(\gamma)$  gives two results!

$$\gamma = \arctan\left(\frac{l_0 - l_2 \sin(\theta)}{l_1 - l_2 \cos(\theta)}\right)$$

Both sin and cosine are negative! Therefore theta should be in the third quadrant.

Add 180 degrees to the equation.

Solving the work done by the user in terms of the angle theta and the force of the user will allow the resistance curve to be graphed. Knowing that  $work = \int F_{user} \dot{\theta} dt$  where  $\dot{\theta} = \frac{d(position\ equation)}{dt}$ . The following calculations solve this.

*Velocity loop equation*

$$\frac{d}{dt} [l_0 \hat{j} - l_1 - l_2 e^{j\theta} - s e^{j\gamma}] = 0$$

$$\dot{\theta} = 0 - 0 - \hat{j} l_2 \dot{\theta} e^{j\theta} - \dot{s} e^{j\gamma} - \hat{j} s \dot{\gamma} e^{j\gamma} = 0 \quad \longleftarrow \quad \text{This uses the FBD above!}$$

$$\dot{\theta} = \hat{j} l_2 \dot{\theta} e^{j\theta} - \dot{s} e^{j\gamma} - \hat{j} s \dot{\gamma} e^{j\gamma}$$

-Expand into RE and IM parts

$$RE: -l_2 \dot{\theta} \sin(\theta) + \dot{s} \cos(\gamma) - s \dot{\gamma} \sin(\gamma) = 0$$

$$IM: l_2 \dot{\theta} \cos(\theta) + \dot{s} \sin(\gamma) - s \dot{\gamma} \cos(\gamma) = 0$$

*Yields: two equations, two unknowns, one known.*

-Substitute the following for ease.

$$A_1 = \cos(\gamma)$$

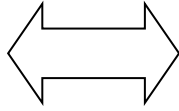
$$A_2 = \sin(\gamma)$$

$$B_1 = -s \sin(\gamma)$$

$$B_2 = s \cos(\gamma)$$

$$C_1 = -l_2 \dot{\theta} \sin(\theta)$$

$$C_2 = l_2 \dot{\theta} \cos(\theta)$$



$$A_1 \dot{s} + B_1 \dot{\gamma} + C_1 = 0$$

$$A_2 \dot{s} + B_2 \dot{\gamma} + C_2 = 0$$

-Solve for  $\dot{s}$  and  $\dot{\gamma}$

$$\dot{s} = \frac{C_1 - B_1 \dot{\gamma}}{A_1}$$

-Therefore

$$A_2 \left[ \frac{C_1 - B_1 \dot{\gamma}}{A_1} \right] + B_2 \dot{\gamma} + C_2 = 0$$

$$\dot{\gamma} = \frac{C_2 + \frac{A_2 C_1}{A_1}}{B_2 - \frac{A_2 B_1}{A_1}}$$

*Virtual Work*

$$F_{user} \dot{\theta} l_3 = F_k \dot{s}$$

$F_{user} = \left( \frac{F_k}{l_3} \right) \left( \frac{\dot{s}}{\dot{\theta}} \right)$  where  $F_k = F_{start} + k\Delta x$  at position  $s$  and where  $\Delta x$  equals *eye-to-eye*

*length* minus  $s$

## Graph Trends

At theta equals 45 degrees, s will be maximum and at 145 degrees, s will be at the eye-to-eye length minus  $\Delta x_{max}$  where  $\Delta x_{max}$  = stroke length.

$$V(45^\circ) = 0 \text{ and } V(125^\circ) = 0$$

$F_{user}$  on the concentric motion should be greater than on the eccentric. This goes against the human strength curve: BAD! To counteract this, a user might be advised to move faster on the outstroke and more slowly on the return stroke.

$$F_{tot} = F_k + k_d V_{xy}(\theta)$$

$$F_{totx} = F_k(s) + k_d V_x(\theta), \quad F_{toty} = F_k(s) + k_d V_y(\theta)$$

$$F_{user(damping)} = \frac{F_{tot(x,y)} \dot{s}}{l_3 \dot{\theta}}$$

## Damping

Damping forces depend on oil viscosity, orifice sizes, piston size, valving, shim configuration and most all, velocity. Damper velocity is how fast the damper compresses or rebounds [32]. For most dampers force is directly proportional to the velocity  $F_d = k_d * V$  where  $k_d$  is the damping coefficient (provided by the manufacturer), and V is the input velocity controlled directly by the user.

$F_{tot} = F_k + F_d = F_k + c\dot{x}$  where  $\dot{x}$  is a function of position which must be graphed in order to find when the velocity ramps up and down and where the peak is located.

## Inertial Force

Inertial force is the second component (first being the resistance of the spring/damping) found in the total users force. This force is generated from the geometry of the exercise machine. This is the concept of reduced mass which is based on the equivalence of kinetic energy in the reduced system and the actual system. The equivalent single mass (or inertia) system is said to be dynamically equivalent to the actual system in the sense that the response of the hypothetical equivalent single mass system to an input force would be identical to the actual multilink system. The actual system of  $n$  members is to be modeled by a single rotating mass of variable moment of inertia,  $I^*$ . At any instant, assuming angular velocity of the mass  $I^*$  as  $\dot{\phi}$ , we equate the kinetic energies of the equivalent systems. (Suh and Radcliffe)

$$\frac{1}{2} I^* \dot{\phi}^2 = \sum_{i=1}^n \frac{1}{2} m_i (\dot{x}_i^2 + \dot{y}_i^2) + \frac{1}{2} I_i \dot{\theta}_i^2$$

-In this case  $\dot{\phi} = \dot{\theta} = 1 \text{ rad/s}$

The above equation must be solved for  $I^*$  in order to solve for  $F_{user}$  in the equation below

$$I^* \ddot{\theta} + F_{user} \dot{\theta} l_3 + F_{spring} \dot{s} = 0$$

*Step 1*- Assume velocity profile based on time and calculate theta double-dot.

1<sup>st</sup> assumed velocity profile: step-up/constant/step-down with an outward stroke total time of .5 seconds.



Define theta total in regards to the outward stroke and then in terms of the area under the assumed velocity curve.

$$\theta_{total} = 125^\circ - 45^\circ = 80^\circ$$

$$\theta_{total} = \frac{1}{2}\dot{\theta}_{max}t_1 + \dot{\theta}_{max}(t_2 - t_1) + \frac{1}{2}\dot{\theta}_{max}(t_t - t_2)$$

-combing the two equations above gives:

$$80^\circ = \dot{\theta}_{max} \left( \frac{-t_1}{2} + \frac{t_2}{2} + \frac{t_t}{2} \right)$$

$$80^\circ = \frac{\dot{\theta}_{max}}{2} (-t_1 + t_2 + t_t)$$

-assuming  $t_t = \frac{1}{2}$  seconds;  $t_1 = \frac{1}{8}$  seconds;  $t_2 = \frac{3}{8}$  seconds

$$\dot{\theta}_{max} = \frac{160}{3/4}$$

Mapping theta domain to time domain allows the user's force in the time domain to be mapped to a time domain with respect to the degree in stroke.

$$\theta_1 = \frac{1}{2}t^2 + C_1 \quad C_1 = 45^\circ$$

$$\theta_2 = \dot{\theta}_{max}t + C_2 \quad C_2 = 58.3333^\circ$$

Note that time starts at zero for each interval

$$\theta_3 = \dot{\theta}_{max}t - \frac{1}{2} \left( \frac{\dot{\theta}_{max}}{t_t - t_2} \right) t_2 + C_2 \quad C_3 = 111.66666^\circ$$

Note that since we start time at t=0 at the beginning of each interval; c<sub>3</sub> will equal the theta in interval 2.

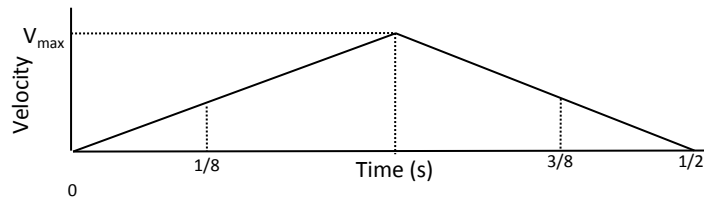
$$\dot{\theta}_{avg} = \frac{\theta_{total}}{\Delta t} = \frac{80^\circ}{1/2} = 160 \frac{^\circ}{s^2}$$

$$\ddot{\theta}_{max} = \frac{\dot{\theta}_{max}}{t_1} = \frac{\dot{\theta}_{max}}{t_t - t_2} = \frac{213}{1/8}$$

-Converting from degree per second square to radians per second square

$$\ddot{\theta}_{max} = 29.7869526$$

2<sup>st</sup> assumed velocity profile: step-up/ step-down with an outward stroke total time of .5 seconds.



Define theta total in regards to the outward stroke and then in terms of the area under the assumed velocity curve.

$$\theta_{total} = 125^\circ - 45^\circ = 80^\circ$$

$$\theta_{total} = \frac{1}{2}\dot{\theta}_{max}(t_2 - t_0) + \frac{1}{2}\dot{\theta}_{max}(t_4 - t_2)$$

-combing the two equations above gives:

$$80^\circ = \dot{\theta}_{max} \left( \frac{1}{8} + \frac{1}{8} \right)$$

$$80^\circ * (4) = \dot{\theta}_{max}$$

-assuming  $t_t = \frac{1}{2}$  seconds;  $t_1 = \frac{1}{8}$  seconds;  $t_2 = \frac{3}{8}$  seconds

$$\dot{\theta}_{max} = 320^\circ/s$$

-mapping theta domain to time domain.

$$\theta_1 = \frac{1}{2} \left( \frac{\dot{\theta}_{max}}{t_2} \right) * t^2 + C_1 \quad C_1 = 45^\circ$$

$$\theta_2 = \dot{\theta}_{max} - \frac{1}{2} \left( \frac{\dot{\theta}_{max}}{t_4 - t_2} \right) t + C_3 \quad C_3 = 85^\circ$$

$$\dot{\theta}_{avg} = \frac{\theta_{total}}{\Delta t} = \frac{80^\circ}{1/2} = 160 \frac{^\circ}{s^2}$$



$$\ddot{\theta}_{max} = \frac{\dot{\theta}_{max}}{t_1} = 22.34 \text{ rad/s}$$

-Converting from degree per second square to radians per second square  $\ddot{\theta}_{max} = 22.34$

### Recap

Use kinematics to find the force needed to compress the spring and moments of inertia to find the force required to move the mass of the structure. Then apply superposition to find the total force. All this will determine if the inertial force is significant and if the user's force curve matches the trend of the human strength curve.

An electrogoniometer was applied to the subject's left knee, centered directly over the rotational joint. The electrogoniometer limits were calibrated for 0° when the user's knee was straight, the top limit equaled 200V, and for 90°, when the knee was bent, the lower limit equaled 0V. The vertical line indicates the maximum voltage of 141.5 at roughly 90 degrees. This curve indicates that the user is generally accelerating or decelerating the foot pedal, with little or no constant velocity in the middle. As a result, the second velocity profile will be assumed for all subsequent analysis. (Results shown in Figure 13 above)

Step 2- solve for moment of inertia (MOI),  $I^*$

Find the volume and mass of each link. Note that these values are the same for links 3 and 4 since they are identical links. Remember to substrate the gaps (no material).

$$V_{link2\_solid} = h * d * w = 6.304 * 5 * 5.23 = 164.85 \text{ cm}^3$$

$$V_{link2\_gaps} = (3.5 * 6.304 * 5.23) = 115.39472 \text{ cm}^3$$

↓ Subtract gaps from solid

$$V_{link2} = 3.0512 \text{ in}^3; M_{link2} = 392.5 \text{ g} = 0.865 \text{ lbs}$$

This mass is both reasonable and realistic.

$$V_{link3\_solid} = h * d * w = 41.91 * 5 * 5.23 = 1095.9465 \text{ cm}^3$$

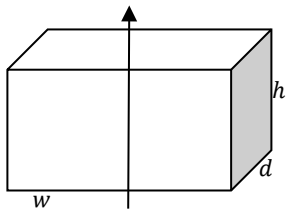
$$V_{link3\_gaps} = (3 * 20.249 * 5.23) + \frac{1}{2}[\pi 1.5^2] * 5.23 = 336.2 \text{ cm}^3$$

↓ Subtract gaps from solid

$$V_{link3} = 46.363 \text{ in}^3; M_{link3} = 5964.05 \text{ g} = 13.15 \text{ lbs}$$

This mass is both reasonable and realistic.

MOI for a cuboid about the cm



$$I_h = \frac{1}{12} m(w^2 + d^2)$$

$$I_w = \frac{1}{12} m(h^2 + d^2)$$

$$I_d = \frac{1}{12} m(h^2 + w^2)$$

The rotation occurs about d. Note that the parallel axis theorem is needed for each link.  $I_z = I_{cm} + mr^2$  where r is the perpendicular distance between the axis of rotation (p) and axis that would pass through the center of mass.

-This yields the following

$$I_{d_{link(2,3,4); \text{ about } p}} = \frac{1}{12} m(h^2 + w^2) + mr^2$$

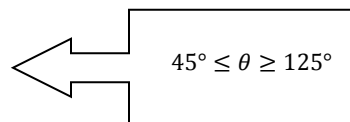
-Sum each for a total inertia force

$$I_{tot} = I_{d_{link2}; \text{ about } p} + I_{d_{link3}; \text{ about } p} + I_{d_{link4}; \text{ about } p} = 3459 \text{ lblb}^2 \text{ or } 1.01 \text{ kgm}^2$$

$$\dot{x} = \dot{\theta} l_3 \cos(90 - \theta)$$

$$\dot{y} = \dot{\theta} l_3 \sin(90 - \theta)$$

$$m = 3.7 \text{ kg or } 8 \text{ lbs}$$



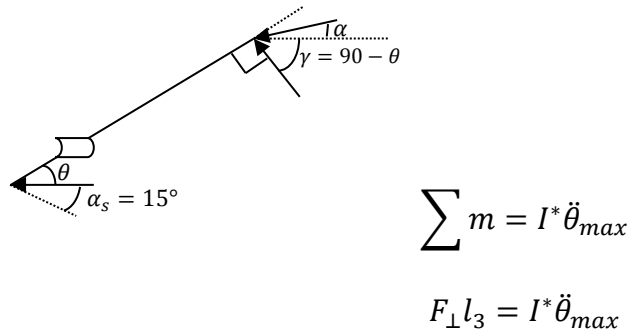
$$I^* = \frac{\frac{1}{2}m(\dot{x}^2 + \dot{y}^2) + \frac{1}{2}I\dot{\theta}^2}{\frac{1}{2}\dot{\theta}^2}$$

↓ Substitute terms

$$I^* = l_3^2 m + I_{tot}$$

The MOI state that the lighter the foot pedal, the less significant the inertial force is. Inertial forces should be minimal so that the resistance curve is closest to the human strength curve. Therefore instead of using a 3.7 kg mass for the pedal (what it weights in steel) assume 1 kg (what it would weight in carbon fibers). This decreases the force required to move the mass of the system.

To find  $F_{user}$  solve for the sum of the moments



From the loop equations  $F_{\perp}$  is known.  $F_{\perp} = F_{user} \cos(\alpha + \gamma)$

$$F_{user} = \frac{F_{\perp}}{\cos(\alpha + \gamma)} = \frac{F_{\perp}}{\cos(25 + (90 - \theta))}$$

# Mechanical Results

Resistance Curve				
Spring Properties		Constant Dimensions (in)		Key
Force (lbs) springs preload	400	L <sub>0</sub>	2	User inputs
Damping coeff. K <sub>d</sub>	2			Results
stroke length (in)	3	L <sub>1</sub>	10.82	
eye to eye length (in)	12.507	L <sub>2</sub> (Center-to-center)	1.95	
k (spring rate)	650	L <sub>3</sub> (end to center)	16	
F <sub>k</sub> (force at s)	=C5*(C3*(C6-E17))			
F <sub>k13</sub> no lever arm	=C10/E9			
K <sub>eff3</sub>	=C6/E9			
Force Spring (lever arm L <sub>2</sub> )	=C10/B27/E22			
Substitutions for γ & s		Variable Dimensions (in)		User force
A <sub>1</sub>	=COS(RADIANS(E16))	α	125	F <sub>user</sub> (lbs) no damping =C17/E22/E20
A <sub>2</sub>	=SIN(RADIANS(E16))	x	=SQRT((E5^2+(E7^2)+(E8^2)*(E7^2)*COS(RADIANS(E16)))+(E5^2)*SIN(RADIANS(E16)))	
B <sub>1</sub>	=-E17*SIN(RADIANS(E16))	y	=DEGREES(ATAN)((E5-(E8^2)*SIN(RADIANS(E16)))/(E7-(E8^2)*COS(RADIANS(E16))))+90	F <sub>user</sub> (lbs) with dampi =F16+(C12*(E22/E20/E22)
B <sub>2</sub>	=E17*COS(RADIANS(E16))	Δα	=C8-E17	
C <sub>1</sub>	=E8^2*27*SIN(RADIANS(E16))	velocity of damper	=1	
C <sub>2</sub>	=E8^2*27*COS(RADIANS(E16))	γ	=(C2+(C17^2*(C20*(C16)/(E17^2)*C16)+C19)	
		s	=(C20-(C16^2)*E21*(C16)	

Figure 23. Resistance curve calculations, implementing the spring properties.

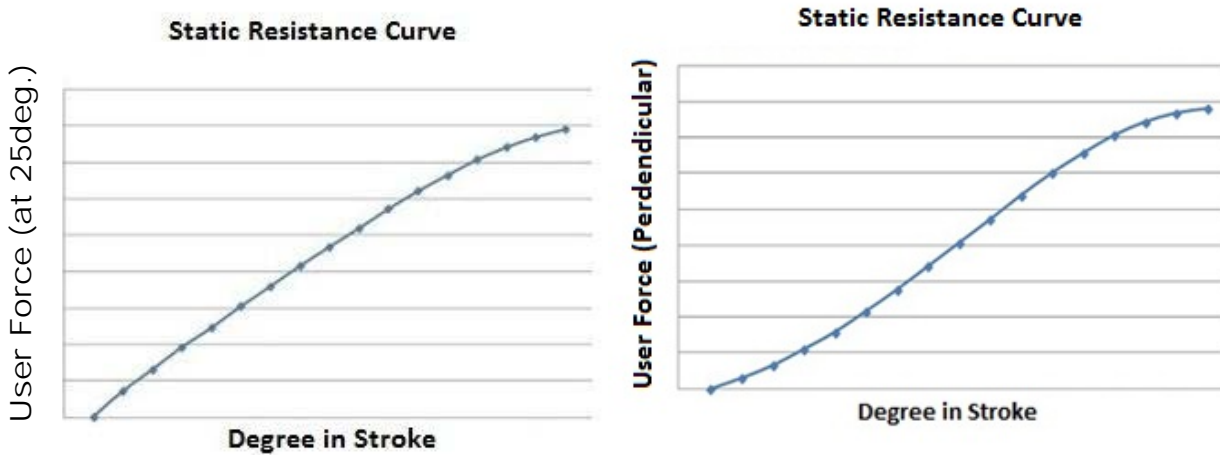


Figure 24. Resistance curve results. (Left), Results for when the user applies a force at a 25° angle relative to the pedal. (Right), Results for when the user applies a force at a 90° degrees angle relative to the pedal. These graphs show that the user force should remain 90° throughout the stroke in order to most closely match the human strength curve.

Virtual Work Solutions					
$\theta$	$s'(\theta)$	$Fk(s)/L3$ (w/o leverarm)	Perpendicular force no damping term	Perpendicular force with damper term	user force at angle 25
45	1.38	=0.04/E9	0	0.24	=Y6/(COS(RADIANS(25)+RADIANS(90-V6)))
50	1.48	=62.57/E9	6	6	=Y7/(COS(RADIANS(25)+RADIANS(90-V7)))
55	1.58	=131.86/E9	13	13.3	=Y8/(COS(RADIANS(25)+RADIANS(90-V8)))
60	1.66	=207.57/E9	22	22	=Y9/(COS(RADIANS(25)+RADIANS(90-V9)))
65	1.74	=289.28/E9	31.5	32	=Y10/(COS(RADIANS(25)+RADIANS(90-V10)))
70	1.81	=376.57/E9	43	43	=Y11/(COS(RADIANS(25)+RADIANS(90-V11)))
75	1.87	=468.93/E9	55	55	=Y12/(COS(RADIANS(25)+RADIANS(90-V12)))
80	1.91	=565.85/E9	68	68	=Y13/(COS(RADIANS(25)+RADIANS(90-V13)))
85	1.94	=666.75/E9	81	85	=Y14/(COS(RADIANS(25)+RADIANS(90-V14)))
90	1.96	=771.01/E9	94	94.8	=Y15/(COS(RADIANS(25)+RADIANS(90-V15)))
95	1.96	=877.96/E9	107.5	108	=Y16/(COS(RADIANS(25)+RADIANS(90-V16)))
100	1.95	=986.88/E9	120	120	=Y17/(COS(RADIANS(25)+RADIANS(90-V17)))
105	1.91	=1097.03/E9	131	132	=Y18/(COS(RADIANS(25)+RADIANS(90-V18)))
110	1.87	=1207.61/E9	141	141.4	=Y19/(COS(RADIANS(25)+RADIANS(90-V19)))
115	1.8	=1317.77/E9	148.5	149	=Y20/(COS(RADIANS(25)+RADIANS(90-V20)))
120	1.72	=1426.63/E9	153.5	154	=Y21/(COS(RADIANS(25)+RADIANS(90-V21)))
125	1.62	=1533.28/E9	156	156	=Y22/(COS(RADIANS(25)+RADIANS(90-V22)))

Figure 25. Virtual work calculations.

Moments of Inertia								
Rod	h (in)	w (in)	d (in)	r (in)	Volume (sq. in.)	mass (lbs) with holes	mass (lbs) w/out holes	MOI (no holes considered)
L2	2.48189	2.05906	1.9685	0.48189	3.0512	0.865	=164.85*7.85*0.00220462	(((1/12)*H27*((B27^2)+(C27^2)))+(H27*(E27^2)))
L3	16.5	2.05906	1.9685	8.25	46.363	13.15	=1095.9465*7.85*0.00220462	(((1/12)*H28*((B28^2)+(C28^2)))+(H28*(E28^2)))
L4	16.5	2.05906	1.9685	8.25	46.363	13.15	=1095.9465*7.85*0.00220462	(((1/12)*H29*((B29^2)+(C29^2)))+(H29*(E29^2)))
Sum of MOI (lb*sq.in)								=I27+I28+I29

Figure 26. Moments of inertia (MOI) calculations assuming the foot pedal is negligible.

MOI Solutions with ramp up, ramp down Vel. Profile									
User just spring full geometry (LBF) Lo = 0.38	User just spring with preload=400lbs full geometry (LBF) Lo = 0.38	User just spring full geometry (LBF) Lo = 1.38	User just spring with preload of 200lbs full geometry (LBF) Lo = 1.38	User just spring with preload of 400lbs full geometry (LBF) Lo = 1.38	User just spring full geometry (LBF) Lo = 2.00	Degree in Stroke	Time Total 5 seconds	zdot	ydot
9.465	41.469	0	17.204	34.478	0	=(640*(T47.2))+45	=0	=(T0.419T COS(RADIANS(90-S47)))	=(T0.419T SIN(RADIANS(90-S47)))
10.251	42.63	0.651	18.054	35.457	0	=(640*(T48.2))+45	=(0.5/16)+T47	=(T0.419T COS(RADIANS(90-S48)))	=(T0.419T SIN(RADIANS(90-S48)))
12.748	46.24	2.723	20.617	38.51	0	=(640*(T49.2))+45	=(0.5/16)+T48	=(T0.419T COS(RADIANS(90-S49)))	=(T0.419T SIN(RADIANS(90-S49)))
17.368	52.683	6.62	25.302	43.984	0	=(640*(T50.2))+45	=(0.5/16)+T49	=(T0.419T COS(RADIANS(90-S50)))	=(T0.419T SIN(RADIANS(90-S50)))
24.877	62.594	13.003	32.725	52.448	2.549	=(640*(T51.2))+45	=(0.5/16)+T50	=(T0.419T COS(RADIANS(90-S51)))	=(T0.419T SIN(RADIANS(90-S51)))
35.15	76.905	22.769	43.709	64.649	11.434	=(640*(T52.2))+45	=(0.5/16)+T51	=(T0.419T COS(RADIANS(90-S52)))	=(T0.419T SIN(RADIANS(90-S52)))
52.417	96.184	36.921	59.145	81.371	24.485	=(640*(T53.2))+45	=(0.5/16)+T52	=(T0.419T COS(RADIANS(90-S53)))	=(T0.419T SIN(RADIANS(90-S53)))
74.452	121.327	56.282	79.694	103.105	42.584	=(640*(T54.2))+45	=(0.5/16)+T53	=(T0.419T COS(RADIANS(90-S54)))	=(T0.419T SIN(RADIANS(90-S54)))
102.35	151.777	80.907	105.176	129.445	65.633	=(640*(T55.2))+45	=(0.5/16)+T54	=(T0.419T COS(RADIANS(90-S55)))	=(T0.419T SIN(RADIANS(90-S55)))
130.631	181.331	109.915	130.418	164.322	89.235	=(320*(T56-0.25))-0.5*(320/(0.5-0.25))*((T56-0.25)^2)/(85)	=(0.5/16)+T55	=(T0.419T COS(RADIANS(90-S56)))	=(T0.419T SIN(RADIANS(90-S56)))
153.171	203.815	125.82	149.973	174.126	108.1	=(320*(T57-0.25))-0.5*(320/(0.5-0.25))*((T57-0.25)^2)/(85)	=(0.5/16)+T56	=(T0.419T COS(RADIANS(90-S57)))	=(T0.419T SIN(RADIANS(90-S57)))
163.144	218.839	139.852	163.282	186.712	121.441	=(320*(T58-0.25))-0.5*(320/(0.5-0.25))*((T58-0.25)^2)/(85)	=(0.5/16)+T57	=(T0.419T COS(RADIANS(90-S58)))	=(T0.419T SIN(RADIANS(90-S58)))
173.122	227.404	148.511	171.051	193.591	129.696	=(320*(T59-0.25))-0.5*(320/(0.5-0.25))*((T59-0.25)^2)/(85)	=(0.5/16)+T58	=(T0.419T COS(RADIANS(90-S59)))	=(T0.419T SIN(RADIANS(90-S59)))
184.49	231.274	153.05	174.711	196.372	131.031	=(320*(T60-0.25))-0.5*(320/(0.5-0.25))*((T60-0.25)^2)/(85)	=(0.5/16)+T59	=(T0.419T COS(RADIANS(90-S60)))	=(T0.419T SIN(RADIANS(90-S60)))
186.866	232.369	154.347	175.882	196.817	135.846	=(320*(T61-0.25))-0.5*(320/(0.5-0.25))*((T61-0.25)^2)/(85)	=(0.5/16)+T60	=(T0.419T COS(RADIANS(90-S61)))	=(T0.419T SIN(RADIANS(90-S61)))
187.664	232.314	155.504	175.364	196.424	136.484	=(320*(T62-0.25))-0.5*(320/(0.5-0.25))*((T62-0.25)^2)/(85)	=(0.5/16)+T61	=(T0.419T COS(RADIANS(90-S62)))	=(T0.419T SIN(RADIANS(90-S62)))
187.821	232.173	155.859	175.884	196.179	136.459	=(320*(T63-0.25))-0.5*(320/(0.5-0.25))*((T63-0.25)^2)/(85)	=(0.5/16)+T62	=(T0.419T COS(RADIANS(90-S63)))	=(T0.419T SIN(RADIANS(90-S63)))

Figure 27. MOI solution for the ramp up, ramp down velocity profile. Calculations the GRF using a zero preload at L<sub>0</sub> equal to two inches. Calculates GRF using 200lb and 400lb spring preload at L<sub>0</sub> equal to 0.38 inches and 1.38 inches.

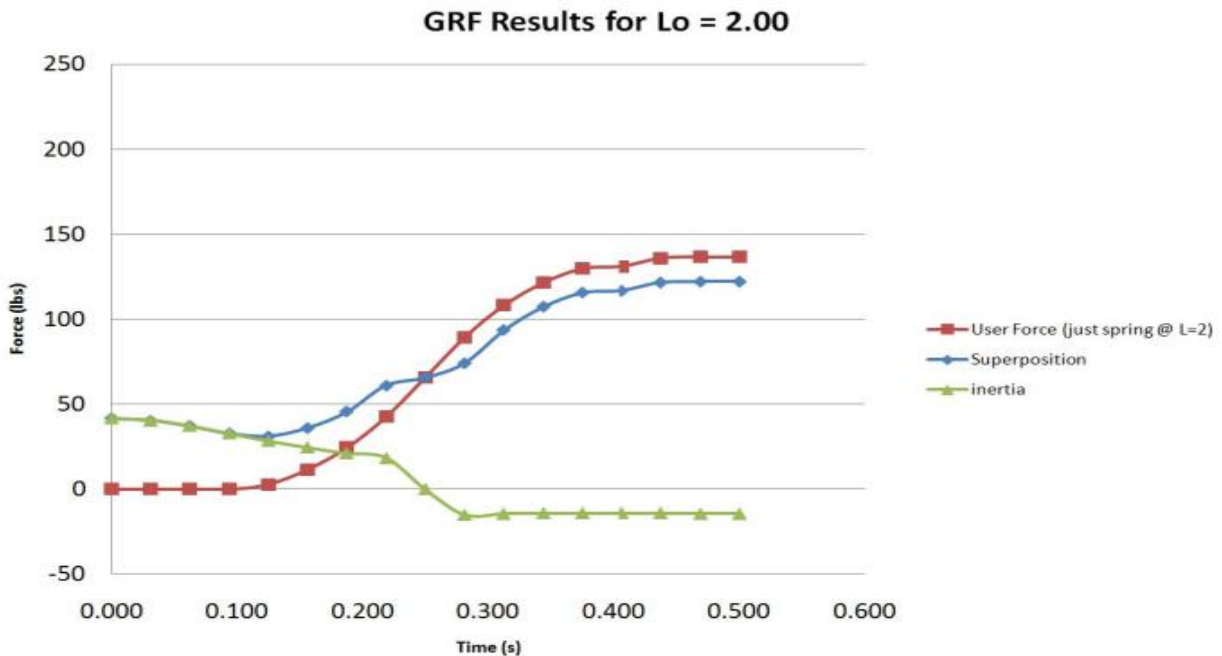


Figure 28. GRF found using a zero spring preload at L<sub>0</sub> equal to two inches assuming ramp up, ramp down velocity profile. Graph displays the total user force required in blue. The green represented the user force required to overcome the geometry of the machine and the blue represented the user force required to overcome the spring resistance.

MOI Solutions with ramp up, ramp down Vel. Profile							
fp	user force, just inertia, full geometry (N)	user force, just inertia, full geometry (LBF)	Superpositio n results for Lo = 0.38 no preload	Superpositi on results for Lo = 0.38 preload 200	Superposition results for Lo = 0.38 preload 400	GRF results for Lo = 0.38 with no preload and A*ΔP=231.35lbf	GRF results for Lo = 0.38 with 400lbs preload and A*ΔP=231.35lbf
=(w47'22.34)(0.4191	=N47(COS(RADIANS(25)+RADIANS(90-S47)))	=0.224808943*(X47(COS(RADIANS(25+(90-S47))))	=Z47+L47	=Z47+P47	=(Z47+M47)	=231.35+(L47+Z47)	=231.35+(M47+Z47)
=(w48'22.34)(0.4191	=N48(COS(RADIANS(25)+RADIANS(90-S48)))	=0.224808943*(X48(COS(RADIANS(25+(90-S48))))	=Z48+L48	=Z48+P48	=(Z48+M48)	=231.35+(L48+Z48)	=231.35+(M48+Z48)
=(w49'22.34)(0.4191	=N49(COS(RADIANS(25)+RADIANS(90-S49)))	=0.224808943*(X49(COS(RADIANS(25+(90-S49))))	=Z49+L49	=Z49+P49	=(Z49+M49)	=231.35+(L49+Z49)	=231.35+(M49+Z49)
=(w50'22.34)(0.4191	=N50(COS(RADIANS(25)+RADIANS(90-S50)))	=0.224808943*(X50(COS(RADIANS(25+(90-S50))))	=Z50+L50	=Z50+P50	=(Z50+M50)	=231.35+(L50+Z50)	=231.35+(M50+Z50)
=(w51'22.34)(0.4191	=N51(COS(RADIANS(25)+RADIANS(90-S51)))	=0.224808943*(X51(COS(RADIANS(25+(90-S51))))	=Z51+L51	=Z51+P51	=(Z51+M51)	=231.35+(L51+Z51)	=231.35+(M51+Z51)
=(w52'22.34)(0.4191	=N52(COS(RADIANS(25)+RADIANS(90-S52)))	=0.224808943*(X52(COS(RADIANS(25+(90-S52))))	=Z52+L52	=Z52+P52	=(Z52+M52)	=231.35+(L52+Z52)	=231.35+(M52+Z52)
=(w53'22.34)(0.4191	=N53(COS(RADIANS(25)+RADIANS(90-S53)))	=0.224808943*(X53(COS(RADIANS(25+(90-S53))))	=Z53+L53	=Z53+P53	=(Z53+M53)	=231.35+(L53+Z53)	=231.35+(M53+Z53)
=(w54'22.34)(0.4191	=N54(COS(RADIANS(25)+RADIANS(90-S54)))	=0.224808943*(X54(COS(RADIANS(25+(90-S54))))	=Z54+L54	=Z54+P54	=(Z54+M54)	=231.35+(L54+Z54)	=231.35+(M54+Z54)
=(w55'0)(0.4191	=N55(COS(RADIANS(25)+RADIANS(90-S55)))	=0.224808943*(X55(COS(RADIANS(25+(90-S55))))	=Z55+L55	=Z55+P55	=(Z55+M55)	=231.35+(L55+Z55)	=231.35+(M55+Z55)
=(w56'22.34)(0.4191	=N56(COS(RADIANS(25)+RADIANS(90-S56)))	=0.224808943*(X56(COS(RADIANS(25+(90-S56))))	=Z56+L56	=Z56+P56	=(Z56+M56)	=231.35+(L56+Z56)	=231.35+(M56+Z56)
=(w57'22.34)(0.4191	=N57(COS(RADIANS(25)+RADIANS(90-S57)))	=0.224808943*(X57(COS(RADIANS(25+(90-S57))))	=Z57+L57	=Z57+P57	=(Z57+M57)	=231.35+(L57+Z57)	=231.35+(M57+Z57)
=(w58'22.34)(0.4191	=N58(COS(RADIANS(25)+RADIANS(90-S58)))	=0.224808943*(X58(COS(RADIANS(25+(90-S58))))	=Z58+L58	=Z58+P58	=(Z58+M58)	=231.35+(L58+Z58)	=231.35+(M58+Z58)
=(w59'22.34)(0.4191	=N59(COS(RADIANS(25)+RADIANS(90-S59)))	=0.224808943*(X59(COS(RADIANS(25+(90-S59))))	=Z59+L59	=Z59+P59	=(Z59+M59)	=231.35+(L59+Z59)	=231.35+(M59+Z59)
=(w60'22.34)(0.4191	=N60(COS(RADIANS(25)+RADIANS(90-S60)))	=0.224808943*(X60(COS(RADIANS(25+(90-S60))))	=Z60+L60	=Z60+P60	=(Z60+M60)	=231.35+(L60+Z60)	=231.35+(M60+Z60)
=(w61'22.34)(0.4191	=N61(COS(RADIANS(25)+RADIANS(90-S61)))	=0.224808943*(X61(COS(RADIANS(25+(90-S61))))	=Z61+L61	=Z61+P61	=(Z61+M61)	=231.35+(L61+Z61)	=231.35+(M61+Z61)
=(w62'22.34)(0.4191	=N62(COS(RADIANS(25)+RADIANS(90-S62)))	=0.224808943*(X62(COS(RADIANS(25+(90-S62))))	=Z62+L62	=Z62+P62	=(Z62+M62)	=231.35+(L62+Z62)	=231.35+(M62+Z62)
=(w63'22.34)(0.4191	=N63(COS(RADIANS(25)+RADIANS(90-S63)))	=0.224808943*(X63(COS(RADIANS(25+(90-S63))))	=Z63+L63	=Z63+P63	=(Z63+M63)	=231.35+(L63+Z63)	=231.35+(M63+Z63)

Figure 29. MOI solution for the ramp up, ramp down velocity profile. Calculates the GRF using zero, 200 lb and 400 lb spring preload at L<sub>o</sub> equal to 0.38 inches and 1.38 inches with 50 mmHg applied.

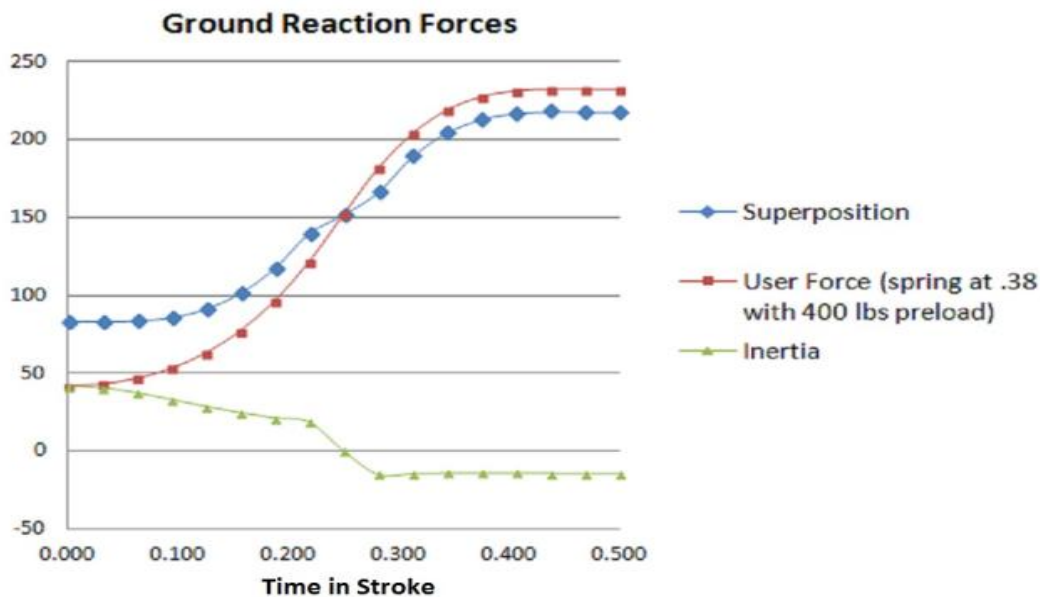


Figure 30. GRF found using a 400 lbs spring preload at L<sub>o</sub> equal to 0.38 inches assuming ramp up, ramp down velocity profile. Graph displays the total user force required in blue. The green represented the user force required to overcome the geometry of the machine and the blue represented the user force required to overcome the spring resistance.

MOI Solutions with ramp up, ramp down Vel. Profile					
GRF results for Lo = 0.38 with 400lbs preload and A*ΔP=231.35lbf	Superposition results for Lo = 1.38	GRF results for Lo = 1.38 with no preload and A*ΔP=231.35lbf	GRF results for Lo = 1.38 with 200lbs preload and A*ΔP=231.35lbf	GRF results for Lo = 1.38 with 400lbs preload and A*ΔP=231.35lbf	Superposition results for Lo = 2.00
=231.35+(M47+Z47)	=N47+Z47	=231.35+(AF47)	=231.35+(Z47+P47)	=231.35+(Z47+Q47)	=Z47+R47
=231.35+(M48+Z48)	=N48+Z48	=231.35+(AF48)	=231.35+(Z48+P48)	=231.35+(Z48+Q48)	=Z48+R48
=231.35+(M49+Z49)	=N49+Z49	=231.35+(AF49)	=231.35+(Z49+P49)	=231.35+(Z49+Q49)	=Z49+R49
=231.35+(M50+Z50)	=N50+Z50	=231.35+(AF50)	=231.35+(Z50+P50)	=231.35+(Z50+Q50)	=Z50+R50
=231.35+(M51+Z51)	=N51+Z51	=231.35+(AF51)	=231.35+(Z51+P51)	=231.35+(Z51+Q51)	=Z51+R51
=231.35+(M52+Z52)	=N52+Z52	=231.35+(AF52)	=231.35+(Z52+P52)	=231.35+(Z52+Q52)	=Z52+R52
=231.35+(M53+Z53)	=N53+Z53	=231.35+(AF53)	=231.35+(Z53+P53)	=231.35+(Z53+Q53)	=Z53+R53
=231.35+(M54+Z54)	=N54+Z54	=231.35+(AF54)	=231.35+(Z54+P54)	=231.35+(Z54+Q54)	=Z54+R54
=231.35+(M55+Z55)	=N55+Z55	=231.35+(AF55)	=231.35+(Z55+P55)	=231.35+(Z55+Q55)	=Z55+R55
=231.35+(M56+Z56)	=N56+Z56	=231.35+(AF56)	=231.35+(Z56+P56)	=231.35+(Z56+Q56)	=Z56+R56
=231.35+(M57+Z57)	=N57+Z57	=231.35+(AF57)	=231.35+(Z57+P57)	=231.35+(Z57+Q57)	=Z57+R57
=231.35+(M58+Z58)	=N58+Z58	=231.35+(AF58)	=231.35+(Z58+P58)	=231.35+(Z58+Q58)	=Z58+R58
=231.35+(M59+Z59)	=N59+Z59	=231.35+(AF59)	=231.35+(Z59+P59)	=231.35+(Z59+Q59)	=Z59+R59
=231.35+(M60+Z60)	=N60+Z60	=231.35+(AF60)	=231.35+(Z60+P60)	=231.35+(Z60+Q60)	=Z60+R60
=231.35+(M61+Z61)	=N61+Z61	=231.35+(AF61)	=231.35+(Z61+P61)	=231.35+(Z61+Q61)	=Z61+R61
=231.35+(M62+Z62)	=N62+Z62	=231.35+(AF62)	=231.35+(Z62+P62)	=231.35+(Z62+Q62)	=Z62+R62
=231.35+(M63+Z63)	=N63+Z63	=231.35+(AF63)	=231.35+(Z63+P63)	=231.35+(Z63+Q63)	=Z63+R63

Figure 31. MOI solution for the ramp up, ramp down velocity profile. Calculates the GRF using 200lb and 400lb spring preload at L<sub>o</sub> equal to 0.38 inches and 1.38 inches with 50 mmHg applied.

MOI Solutions with ramp up, constant, ramp down Vel. Profile							
gdot	l' m=ikg	fp just inertia (N)	user force, just inertia, full geometry (N)	user force, just inertia, full geometry (LBF)	Superposition results for Lo = 0.38	Superposition results for Lo = 0.38 preload 200	Superposition results for Lo = 0.38 preload 400
=T0.4191*SIN(RADIANS(90-S27))	=0.419T2*(l)+1.01	=(w27*29.7869526)/0.4191	=X27(COS(RADIANS(25)+RADIANS(90-S27)))	=0.224808943*(X27(COS(RADIANS(25+(90-S27))))	=Z27+L27	=Z27+P27	=(Z27+M27)
=T0.4191*SIN(RADIANS(90-S28))	=0.419T2*(l)+1.01	=(w28*29.7869526)/0.4191	=X28(COS(RADIANS(25)+RADIANS(90-S28)))	=0.224808943*(X28(COS(RADIANS(25+(90-S28))))	=Z28+L28	=Z28+P28	=(Z28+M28)
=T0.4191*SIN(RADIANS(90-S29))	=0.419T2*(l)+1.01	=(w29*29.7869526)/0.4191	=X29(COS(RADIANS(25)+RADIANS(90-S29)))	=0.224808943*(X29(COS(RADIANS(25+(90-S29))))	=Z29+L29	=Z29+P29	=(Z29+M29)
=T0.4191*SIN(RADIANS(90-S30))	=0.419T2*(l)+1.01	=(w30*29.7869526)/0.4191	=X30(COS(RADIANS(25)+RADIANS(90-S30)))	=0.224808943*(X30(COS(RADIANS(25+(90-S30))))	=Z30+L30	=Z30+P30	=(Z30+M30)
=T0.4191*SIN(RADIANS(90-S31))	=0.419T2*(l)+1.01	=(w31*29.7869526)/0.4191	=X31(COS(RADIANS(25)+RADIANS(90-S31)))	=0.224808943*(X31(COS(RADIANS(25+(90-S31))))	=Z31+L31	=Z31+P31	=(Z31+M31)
=T0.4191*SIN(RADIANS(90-S32))	=0.419T2*(l)+1.01	0	=X32(COS(RADIANS(25)+RADIANS(90-S32)))	=0.224808943*(X32(COS(RADIANS(25+(90-S32))))	=Z32+L32	=Z32+P32	=(Z32+M32)
=T0.4191*SIN(RADIANS(90-S33))	=0.419T2*(l)+1.01	0	=X33(COS(RADIANS(25)+RADIANS(90-S33)))	=0.224808943*(X33(COS(RADIANS(25+(90-S33))))	=Z33+L33	=Z33+P33	=(Z33+M33)
=T0.4191*SIN(RADIANS(90-S34))	=0.419T2*(l)+1.01	0	=X34(COS(RADIANS(25)+RADIANS(90-S34)))	=0.224808943*(X34(COS(RADIANS(25+(90-S34))))	=Z34+L34	=Z34+P34	=(Z34+M34)
=T0.4191*SIN(RADIANS(90-S35))	=0.419T2*(l)+1.01	0	=X35(COS(RADIANS(25)+RADIANS(90-S35)))	=0.224808943*(X35(COS(RADIANS(25+(90-S35))))	=Z35+L35	=Z35+P35	=(Z35+M35)
=T0.4191*SIN(RADIANS(90-S36))	=0.419T2*(l)+1.01	0	=X36(COS(RADIANS(25)+RADIANS(90-S36)))	=0.224808943*(X36(COS(RADIANS(25+(90-S36))))	=Z36+L36	=Z36+P36	=(Z36+M36)
=T0.4191*SIN(RADIANS(90-S37))	=0.419T2*(l)+1.01	0	=X37(COS(RADIANS(25)+RADIANS(90-S37)))	=0.224808943*(X37(COS(RADIANS(25+(90-S37))))	=Z37+L37	=Z37+P37	=(Z37+M37)
=T0.4191*SIN(RADIANS(90-S38))	=0.419T2*(l)+1.01	0	=X38(COS(RADIANS(25)+RADIANS(90-S38)))	=0.224808943*(X38(COS(RADIANS(25+(90-S38))))	=Z38+L38	=Z38+P38	=(Z38+M38)
=T0.4191*SIN(RADIANS(90-S39))	=0.419T2*(l)+1.01	0	=X39(COS(RADIANS(25)+RADIANS(90-S39)))	=0.224808943*(X39(COS(RADIANS(25+(90-S39))))	=Z39+L39	=Z39+P39	=(Z39+M39)
=T0.4191*SIN(RADIANS(90-S40))	=0.419T2*(l)+1.01	=(w40*29.7869526)/0.4191	=X40(COS(RADIANS(25)+RADIANS(90-S40)))	=0.224808943*(X40(COS(RADIANS(25+(90-S40))))	=Z40+L40	=Z40+P40	=(Z40+M40)
=T0.4191*SIN(RADIANS(90-S41))	=0.419T2*(l)+1.01	=(w41*29.7869526)/0.4191	=X41(COS(RADIANS(25)+RADIANS(90-S41)))	=0.224808943*(X41(COS(RADIANS(25+(90-S41))))	=Z41+L41	=Z41+P41	=(Z41+M41)
=T0.4191*SIN(RADIANS(90-S42))	=0.419T2*(l)+1.01	=(w42*29.7869526)/0.4191	=X42(COS(RADIANS(25)+RADIANS(90-S42)))	=0.224808943*(X42(COS(RADIANS(25+(90-S42))))	=Z42+L42	=Z42+P42	=(Z42+M42)
=T0.4191*SIN(RADIANS(90-S43))	=0.419T2*(l)+1.01	=(w43*29.7869526)/0.4191	=X43(COS(RADIANS(25)+RADIANS(90-S43)))	=0.224808943*(X43(COS(RADIANS(25+(90-S43))))	=Z43+L43	=Z43+P43	=(Z43+M43)

Figure 32. MOI solution for the ramp up, constant, ramp down velocity profile.

Calculations for the GRF using 200 lb and 400 lb spring preload at L<sub>o</sub> equal to 0.38 inches.



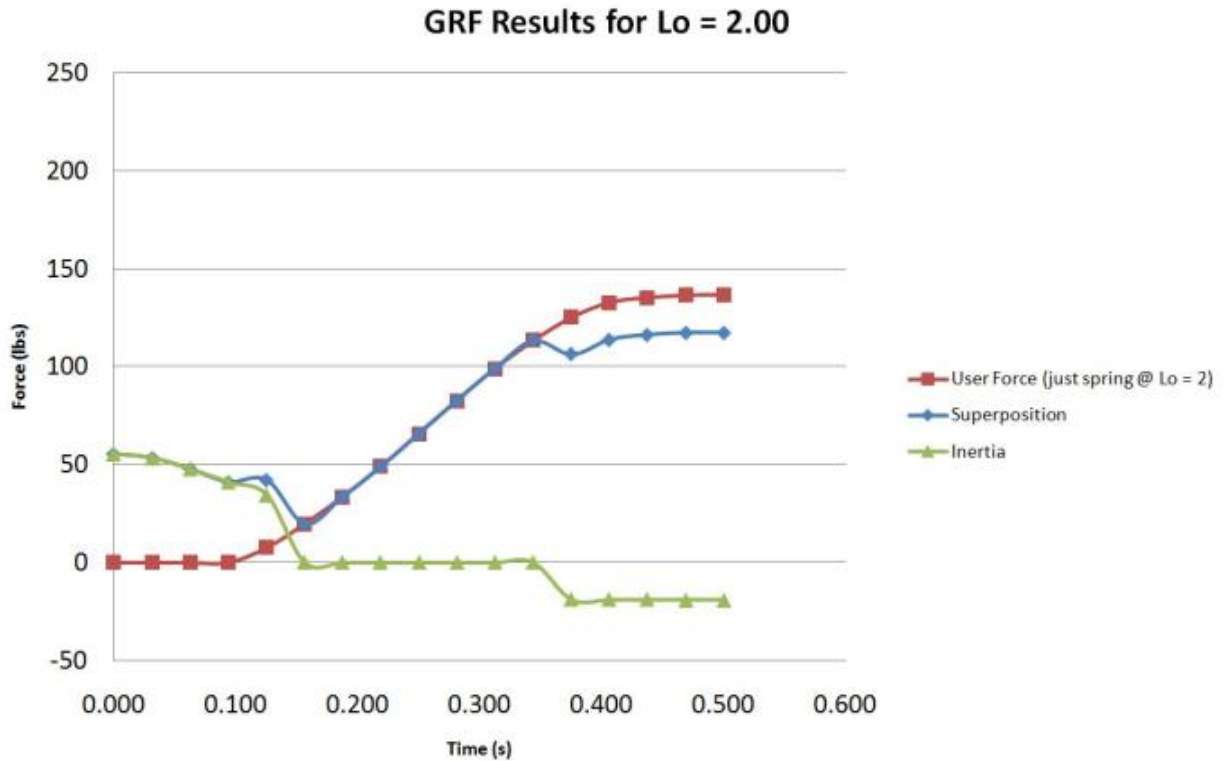


Figure 33. GRF found using a zero spring preload at  $L_0$  equal to two inches assuming ramp up, constant, ramp down velocity profile. Graph displays the total user force required in blue. The green represented the user force required to overcome the geometry of the machine and the blue represented the user force required to overcome the spring resistance.



MOI Solutions with ramp up, constant, ramp down Vel. Profile						
GRF results for Lo = 0.38 with no preload and A*ΔP=231.35lbf	GRF results for Lo = 0.38 with 400lbs preload and A*ΔP=231.35lbf	Superpositio n results for Lo = 1.38	GRF results for Lo = 1.38 with no preload and A*ΔP=231.35lbf	GRF results for Lo = 1.38 with 200lbs preload and A*ΔP=231.35lbf	GRF results for Lo = 1.38 with 400lbs preload and A*ΔP=231.35lbf	Superpositio n results for Lo = 2.00
=231.35+Z27+L27	=231.35+Z27+M27	=N27+Z27	=231.35+(AF27)	=231.35+Z27+P27	=231.35+Z27+Q27	=Z27+R27
=231.35+Z28+L28	=231.35+Z28+M28	=N28+Z28	=231.35+(AF28)	=231.35+Z28+P28	=231.35+Z28+Q28	=Z28+R28
=231.35+Z29+L29	=231.35+Z29+M29	=N29+Z29	=231.35+(AF29)	=231.35+Z29+P29	=231.35+Z29+Q29	=Z29+R29
=231.35+Z30+L30	=231.35+Z30+M30	=N30+Z30	=231.35+(AF30)	=231.35+Z30+P30	=231.35+Z30+Q30	=Z30+R30
=231.35+Z31+L31	=231.35+Z31+M31	=N31+Z31	=231.35+(AF31)	=231.35+Z31+P31	=231.35+Z31+Q31	=Z31+R31
=231.35+Z32+L32	=231.35+Z32+M32	=N32+Z32	=231.35+(AF32)	=231.35+Z32+P32	=231.35+Z32+Q32	=Z32+R32
=231.35+Z33+L33	=231.35+Z33+M33	=N33+Z33	=231.35+(AF33)	=231.35+Z33+P33	=231.35+Z33+Q33	=Z33+R33
=231.35+Z34+L34	=231.35+Z34+M34	=N34+Z34	=231.35+(AF34)	=231.35+Z34+P34	=231.35+Z34+Q34	=Z34+R34
=231.35+Z35+L35	=231.35+Z35+M35	=N35+Z35	=231.35+(AF35)	=231.35+Z35+P35	=231.35+Z35+Q35	=Z35+R35
=231.35+Z36+L36	=231.35+Z36+M36	=N36+Z36	=231.35+(AF36)	=231.35+Z36+P36	=231.35+Z36+Q36	=Z36+R36
=231.35+Z37+L37	=231.35+Z37+M37	=N37+Z37	=231.35+(AF37)	=231.35+Z37+P37	=231.35+Z37+Q37	=Z37+R37
=231.35+Z38+L38	=231.35+Z38+M38	=N38+Z38	=231.35+(AF38)	=231.35+Z38+P38	=231.35+Z38+Q38	=Z38+R38
=231.35+Z39+L39	=231.35+Z39+M39	=N39+Z39	=231.35+(AF39)	=231.35+Z39+P39	=231.35+Z39+Q39	=Z39+R39
=231.35+Z40+L40	=231.35+Z40+M40	=N40+Z40	=231.35+(AF40)	=231.35+Z40+P40	=231.35+Z40+Q40	=Z40+R40
=231.35+Z41+L41	=231.35+Z41+M41	=N41+Z41	=231.35+(AF41)	=231.35+Z41+P41	=231.35+Z41+Q41	=Z41+R41
=231.35+Z42+L42	=231.35+Z42+M42	=N42+Z42	=231.35+(AF42)	=231.35+Z42+P42	=231.35+Z42+Q42	=Z42+R42
=231.35+Z43+L43	=231.35+Z43+M43	=N43+Z43	=231.35+(AF43)	=231.35+Z43+P43	=231.35+Z43+Q43	=Z43+R43

Figure 36. MOI solution for the ramp up, constant, ramp down velocity profile. Calculates the GRF using zero, 200 lb and 400 lb spring preload at  $L_o$  equal to 0.38 inches and 1.38 inches with 50 mmHg applied.

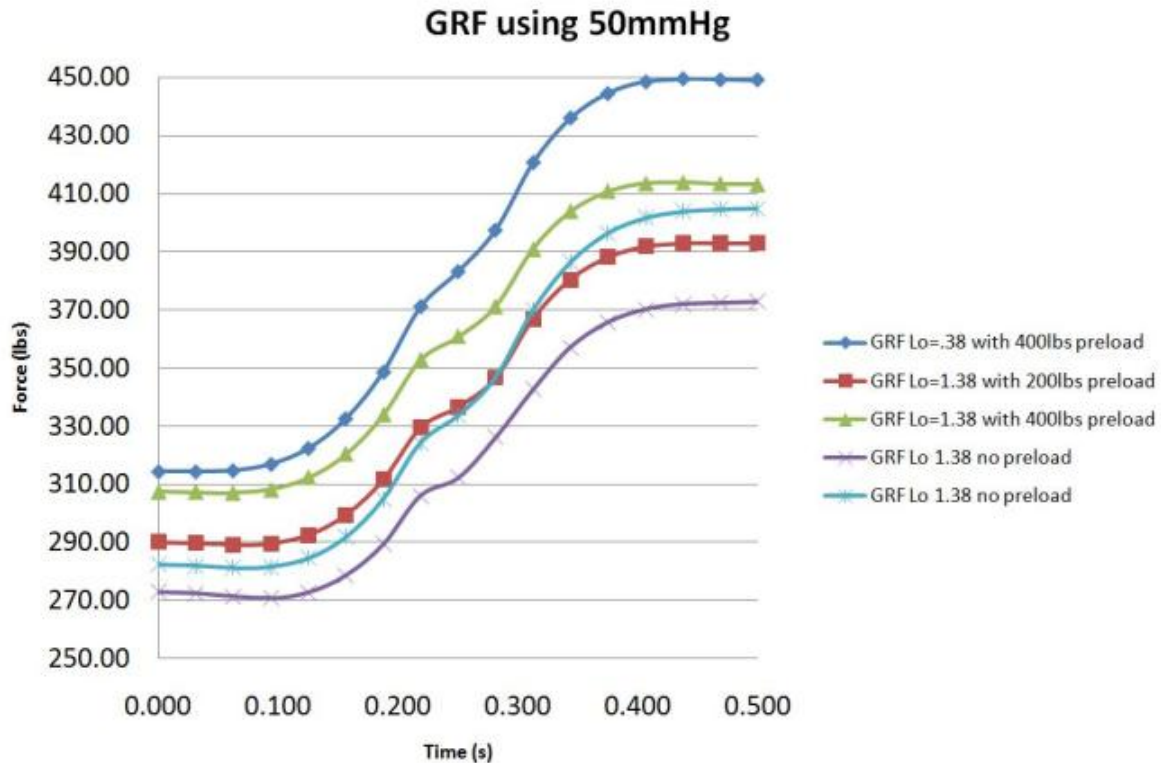


Figure 37. GRF found using a 0 lb, 200 lb, and 400 lb spring preload at  $L_0$  equal to 0.38 inches, and 1.38 inches assuming ramp up, constant, ramp down velocity profile with 50 mmHg applied.

## Physiological Results

The physiological and biomechanical responses of each subject during the protocol will evaluate the positive physiological adaptations achieved through the combination of exercise and LBNP. Each subject throughout the protocol, to ensure safety, had their blood pressure, blood flow and respiratory and cardiovascular responses measured using automatic pulse monitor (HEM-631INT, Omron, co), Doppler ultrasound (LOGIQ Book XP, GE Health Care), a gas analyzer VO2000 (Medical Graphics Corporation), and 12-lead Micromed Digital Electrocardiogram (Micromed Biotechnology Inc.) paired with a Polar heart rate monitor strap, respectfully. The heart rate (HR) levels

shown in Figure 38, from initial testing, indicate that the exercise is non-cardio within the first 3 minutes. However the HR of each subject increased with time. With more time it is believed, based off the Borg scale results, shown in Figure 39, that the HR would reach a cardio state.

Heart Rate 60% Level of Intesity												
Subject	Supine						Upright					
	rest	1st minute	2nd minute	3rd minute	Recovery Time	Target HR	rest	1st minute	2nd minute	3rd minute	Recovery Time	Target HR
1	N/A	N/A	N/A	N/A	N/A	N/A	80	115	122	132	0:02:40	164
2	74	105	108	109	0:01:40	161.6	81	111	127	131	0:05:16	164.4
3	77	122	120	120	0:02:20	162.8	77	106	120	118	0:01:30	162.8
4	74	117	113	109	0:02:40	161.6	70	115	114	108	0:01:50	160

Figure 38. Recorded heart rate levels for 4 subjects using the initial protocol at preliminary stages of testing. Later testing showed high cardio levels when stiffer spring was used.

Borg's Scale 6-20 Level of Intesity						
Subject	Supine			Upright		
	After 1st minute	After 2nd minute	after 3rd minute	After 1st minute	After 2nd minute	after 3rd minute
1	15	17	19	11	11	13
2	8	11	13	11	13	14
3	12	16	18	11	12	13
4	12	12	13	10	12	12
Median	12.0	14.0	15.5	11.0	12.0	13.0
Std. Dev.	2.9	2.9	3.2	0.5	0.8	0.8
			3rd minute supine	15.5	80% effort	

Figure 39. Each subject pointed to a number on the Borg's scale that correlated to the intensity level of the workout.

The muscle activity in the femoris, vastus lateralis, gastrocnemius medial head and soleus will be monitored by a four channel electromyography (EMG) Miotool 400

(Miotec Biomedical Equipments) with an applied gain of 100 in 4 channels, and a band pass filter of 20-450Hz with a first-order Butterworth. The techniques of electromyography follow the recommendations of SENIAM (Surface Electromyography for the Non-invasive Assessment of Muscles). The results are listed below.

EMG Results																
Subject	Supine								Upright							
	TA		RF		BF		GM		TA		RF		BF		GM	
	Max.	CVM	Max.	CVM	Max.	CVM	Max.	CVM	Max.	CVM	Max.	CVM	Max.	CVM	Max.	CVM
1	246.8	208.8	316.1	343.8	1021	327.9	434	120.7	573.5	248.9	512.7	377.1	261	81.7	383.7	51.8
5	238.8	623.8	178.7	131.9	721.5	377.3	506.8	277.8	325.8	52.8	329.2	368.9	236.6	183.9	851.5	615.7
6	235.6	35.1	115.7	143.2	415.8	80.9	269.2	295.7	692.1	193	484.4	143.2	451.2	236.6	252.5	79.2

Figure 40. Recorded electromyography results for 3 subjects. These tests were both preliminary and inconclusive.

The team realized that the muscles that where most curtail to this study where the rectus femoris, long head, vastus medialis, vastus lateralis, Semitendinosus, and Gastrocnemius Medialis. The similar muscle activity shown in the upright versus supine position (*shown below, respectfully*) is a key indicator that this machine can be a success in both environments when paired with differential pressure.

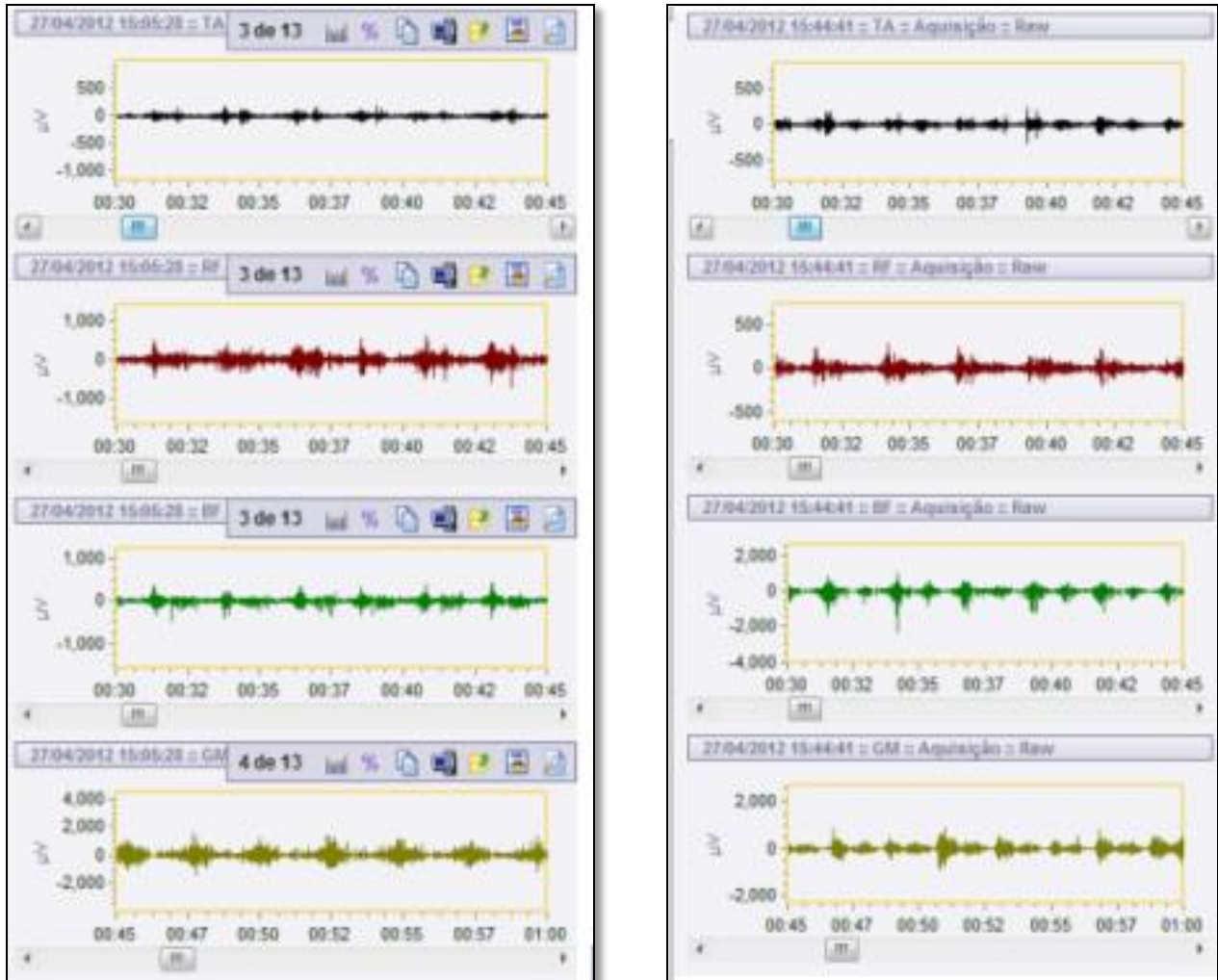


Figure 41. Muscle activity shown in the upright (left) versus supine (right) position.

The code required to find the maximum, minimum voltage of the EMG signals which would allow researchers to compare the EMG Graph and resistance curve in relations is stated below (calculations were done in Matlab)

```
clear all;
close all;
prompt = ('Digite o diretório onde encontram-se os arquivos a serem analisados:');
caminho = inputdlg(prompt);
addpath = caminho;

data = uigetfile('*.txt','Selecione o arquivo de dados:');
dados = load(data);
vetor = dados';
```

```

abs_vector = abs (vetor);
vetor_final = abs_vector;

prompt = ('Digite o limite inferior do sinal (repouso):');
low = input(prompt); %define "low" como o limite inferior para cortar os dados

length = length(abs_vector);
low_vector = [1:1:length];
low_vector = low_vector./low_vector;

low_vector = low_vector*low;
b = abs_vector > low_vector;
vetor_final = abs_vector(logical(b));

max = max(vetor_final)
min = min(vetor_final)
average = mean(vetor_final)
standard_deviation = std(vetor_final)
variance = var(vetor_final);

```

The ground reaction forces, given more time, would be continuously measured by using a pressure distribution Insole (Pedar-System, Novel GmbH, Germany). The force measured by the force insole was calibrated in the x-axis with an Alfa Instruments load cell (Mod.1) and my PCLab data acquisition tool. The testing was cut after only two test due to the owner falling ill.



*Figure 42.* pressure distribution Insole that measured the ground reaction force for each subject.





Figure 43. Subject being fitted for the pressure distribution insole that measures ground reaction force.

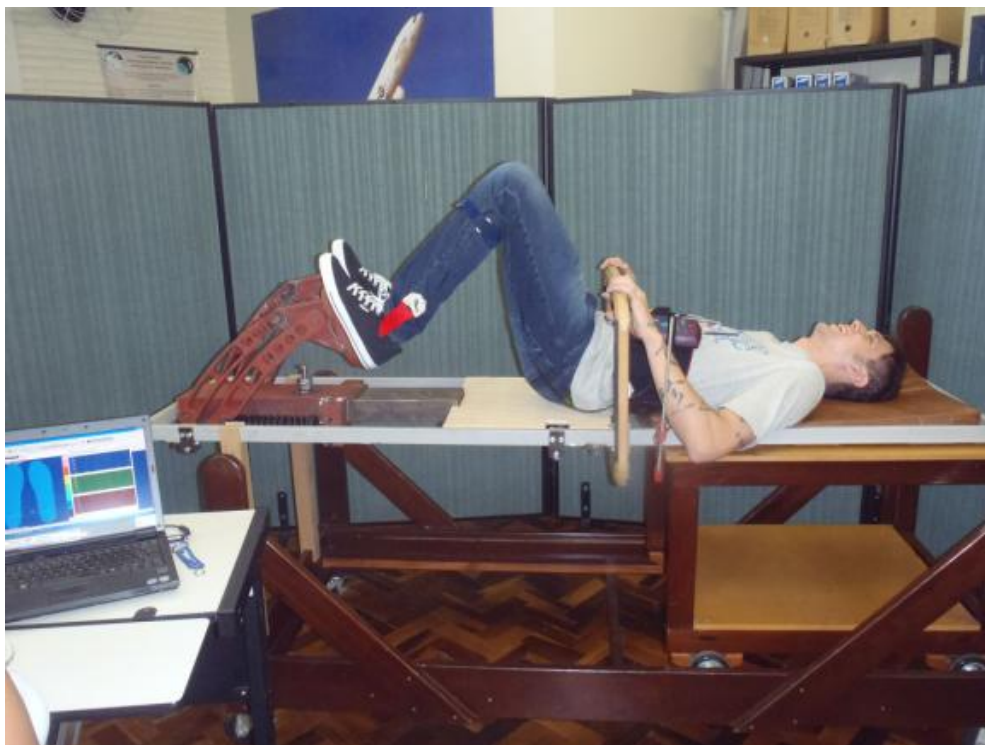


Figure 44. Subject testing the insole.

## Preliminary kinematic problems and solutions

The design process started with a simple 2-D sketch shown in Figure 3, it was then designed as a 3-D CAD model, followed by three prototypes.

The first prototype showed a problem of over-died-center in regards to the spring. This was corrected by linearly aligning all three joints of rotation shown in figure 43.

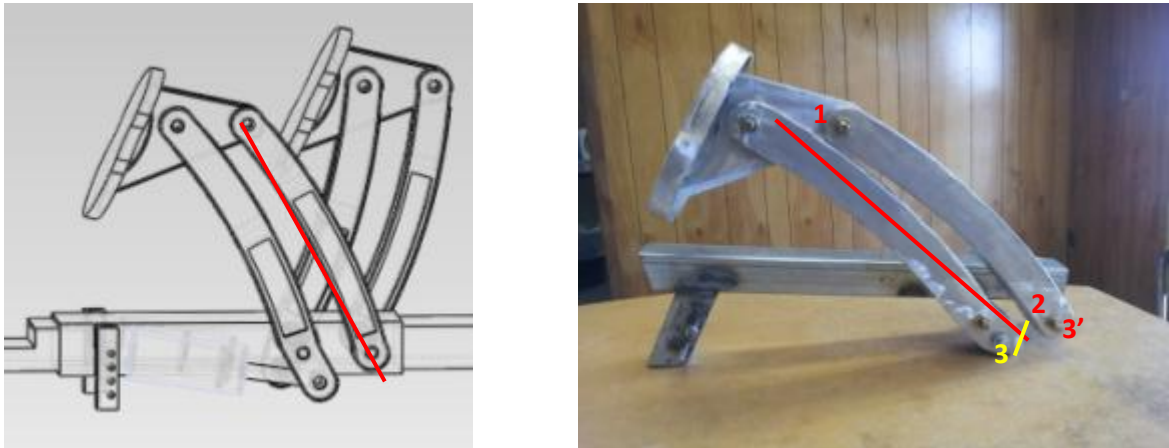


Figure 45. 3-D CAD model displays three rotational joints linearly aligned shown on the left. In the first prototype, shown on the right, joint 3 (shown in yellow) was offset from the line connecting joints 1 and 2. This design proved problematic because the spring moved through the over-died-center. The problem was corrected by moving the 3rd rotational point in line with joints 1 and 2. This is shown in red.

During the second prototype it was noticed that the existing trolley supports prevented the pedals from moving freely throughout their entire rotation. This was solved by relocating the horizontal supports toward the far extremes of the trolley giving the multi-platform enough room to be fully maneuverable.



Figure 46. second prototype mated to the existing trolley, shown on the left, after the horizontal supports were relocated. The 2nd prototype mated to the existing LBNP box, shown on the right.

After testing the third prototype, it was found that the angle of the foot pedal needs to be adjusted so that the user's foot maintains an angle closer to  $90^\circ$  throughout the entire cycle rather than just toward the beginning and the end of the stroke. Currently, too much of the force from the subject's foot is directed along the link, resulting in user forces that are somewhat higher than desired for the first half of the pedal stroke.

## References

1. Boda, Wanda L., Donald E. Watenpaugh, Richard E. Ballard, and Alan R. Hargens. (2000).

"Supine lower body negative pressure exercise simulates metabolic and kinetic features of upright exercise ." *Journal of Applied Physiology*. 89, 218-227

2. Caillot-Augusseau A, Lafage-Proust M-H, Soler C, Pernod J, Dubois F & Alexandre C. (1998).

Bone formation and resorption biological markers in cosmonauts during and after a 180-day space flight (Euromir 95). *Clinical Chemistry* 44, 578-585.

3. Charles, J. B. and Lathers, C. M. (1991).

Cardiovascular Adaptation to Spaceflight. *Journal of Clinical Pharma*, 31: 1010–1023. doi: 10.1002/j.1552-4604.1991.tb03665.x

4. Davis BL and Cavanaugh PR. (1993).

Simulating reduced gravity: a review of biomechanical issues pertaining to human motion. *Aviation Space Environ Med* 64: 557–566, 1993.

5. Convertino VA & Cooke WH. (2005).

Evaluation of Cardiovascular Risks of Spaceflight Does Not Support the NASA Bioastronautics Critical Path Roadmap. *Aviation, Space, and Environmental Medicine* 76, 869-876.

6. Lang T, LeBlanc A, Evans H, Lu Y, Genant H & Yu A. (2004).

Cortical and Trabecular Bone Mineral Loss From the Spine and Hip in Long-Duration Spaceflight. *Journal of Bone and Mineral Research* 19, 1006-1012.

7. Shackelford, LC (2008).

Musculoskeletal response to space flight, pp. 293-306. New York (NY): Oxford University Press, *Principles of clinical medicine for space flight*.

8. Hall, A.S., 1961,

*Kinematics and Linkage Design*, Prentice-Hall, Englewood Cliffs, NJ, pp.4, 47

9. Gazenko OG, Gurovsky NN, Genin AM, Bryanov II, Eryomin AV, and Egorov AD. (1976).

Results of medical investigations carried out on board the Salyut orbital stations. *Life Science* 14:145–152.

10. Bokelberg, E. H., and Gilmore, B. J., 1990.

“A kinematic Design Methodology for exercise/Rehabilitation Machines Using Springs and Mechanical Advantage to Provide Variable Resistance,” *Flexible Mechanism, dynamic and robotic trajectories*, Proceedings 21st Biennial Mechanism Conference, ASME, New York, pp. 279-286.

11. Russomano T, Falcão F, Gurgel J, Piccoli L, Porto F, Dalmarco G, et al. In. (2005).

Development of a lower body negative pressure box with an environmental control system for physiological studies. Annual international conference of the IEEE engineering in medicine and biology - proceedings 4501-4,

12. Tidwell, P. H., Bandukwala, N., Dhande, S. G., Reinholtz, C. F. and Webb, G., (1994).

"Synthesis of Wrapping Cams," *Journal of Mechanical Design*, ASME Transactions, Vol. 116, No. 2, pp. 634-638.

13. Scardina, M.T., Soper, R. R., Calkins, J. M. and Reinholtz, C. F., (1995).

"Optimal Synthesis of Force-Generating Planar Four-Link Mechanisms,"  
Proceedings of the 4th National Applied Mechanisms and Robotics Conference,  
Cincinnati, Ohio, Paper AMR 95-003.

14. Soper, R. R., Scardina, M., Tidwell, P., Reinholtz, C. F. and Lo Presti M. A., (1995).

"Closed-Form Synthesis of Force-Generating Planar Four-Bar Linkages,"  
DE-Vol. 82, Advances in Design Automation, Proceedings of the 1995 ASME Design  
Technical Conferences, Boston, MA, pp. 845-851.

15. Tidwell, P. H., Soper, R. R., and Reinholtz, C. F., (1996).

"Synthesis of Force-Generating Mechanisms," Proceedings of the 24th Biennial  
Mechanisms Conference, Irvine, California, August 18-22, paper 96-DETC/MECH-1211.

16. Vorobyev YI, Gazenko OG, Gurovskiy NN, Nefedov YG, Yegorov BB, Bayevskiy RM,  
Bryanov II, Genin AM, Degtyarev VA, Yegorov AD, Yereimin AV, and Pestov ID. (1976).

Preliminary results of medical investigations carried out during flight of the second  
expedition of the Salyut-4 orbital station. Kosm Biol Aviakosm Med 10: 3–18.

17. Watenpaugh DE and Hargens AR. (1996).

The cardiovascular system in microgravity. In: Handbook of Physiology.  
Environmental Physiology. Bethesda, MD: Am. Physiol. Soc., 1996, sect. 4, vol. I, chapt.  
29, p. 631–674.

18. Brian W. Schulz, Stephanie Hart-Hughes, Mark T. Gordon, Tatjana Bulat,

"Training implications of maximal forces on a computer-controlled and  
motor-driven leg press by age group, sex, footplate direction, and speed," Experimental  
Gerontology, Volume 47, Pages 295-303, ISSN 0531-5565,

10.1016/j.exger.2012.01.003.(<http://www.sciencedirect.com/science/article/pii/S0531556512000162>)

19. Brian W. Schulz, Stephanie Hart-Hughes, Mark T. Gordon, Tatjana Bulat (2012)  
Experimental Gerontology, Volume 47, Issue 4, Pages 295–303

20. Gianoudis, Jenny , Christine Bailey, Sanders Kerrie, Nowson Caryl, Hill Keith ,  
Ebeling Peter , and Daly Robin. (2012)

"BMC Musculoskeletal Disorders." *Protocol for a community-based randomised controlled trial of a multi-modal exercise and osteoporosis education program for older adults at risk of falls and fractures*. BioMed Central, 28 may 1212. Web. 21.

<<http://www.biomedcentral.com/1471-2474/13/78>>.

21. Suh, C. H, and , Radcliffe, C. W.,

"Kinematics and Mechanisms Design," R.E. Krieger Pub. Co., 1978 - 434 pages

22. Sara R. Zwart, Alan R. Hargensb, Stuart M.C. Leec, Brandon R. Maciasb, Donald E.  
Watenpaughd, Kevin Tseb, Scott M. Smithe, (2007)

Bone Volume 40, Issue 2, Pages 529–537

23. Obama, Barack.

"Fiscal year 2012 budget of the U.S. Government."

<http://www.whitehouse.gov/omb/>. N.p., 14 feb 2011.

24. Roberts, MD, James R..

"Overview of Fractures." The Merck Manual Home Health Handbook. N.p., n.d.

<[http://www.merckmanuals.com/home/injuries\\_and\\_poisoning/fractures/overview\\_of\\_fractures.html](http://www.merckmanuals.com/home/injuries_and_poisoning/fractures/overview_of_fractures.html)>.

25. Scheve, Tom.

"How Bones Work" 10 February 2009. HowStuffWorks.com.

<<http://science.howstuffworks.com/life/human-biology/bone.htm>> 05 April 2013.

26. Kalapatapu, MD, Venkat .

"Lower extremity amputation." Wolters Kluwer Health. N.p., 1 june 2012.

27. Roy, Steve.

"How Long Does It Take to Rebuild Bone Lost During Space Flight." NASA. NASA, Marshall Space Flight Center, 26 02 2007. Web. 5 Apr 2013.

<[http://www.nasa.gov/mission\\_pages/station/research/subregional\\_bone.html](http://www.nasa.gov/mission_pages/station/research/subregional_bone.html)>.

28. "TYPE 2 DIABETES AND AMPUTATION." Insulite Laboratories. Insulite Laboratories Medical & Advisory Board. Web.

<<http://diabetesmanagement.insulitelabs.com/index.php?q=type-2-diabetes-and-amputation.php>>.

29. "War Veterans Recover at Brooke Army Medical Center." Big Picture. (2012): n. page. Web. 5 Apr. 2013.

<[http://www.boston.com/bigpicture/2012/08/war\\_veterans\\_recover\\_at\\_brooke.html](http://www.boston.com/bigpicture/2012/08/war_veterans_recover_at_brooke.html)>.

30. "Duchess of Cornwall visits military rehab centre." Telegraph. (2009): n. page. Web. 5 Apr. 2013.

31. Hsu, Jeremy.

"Great NASA Tech Spinoffs Come Down to Earth." Space.com. 23 nov 2009: n. page. Print. <<http://www.space.com/7556-great-nasa-tech-spinoffs-earth.html>>.

32. "Damping." Wikipedia. 2013. <<http://en.wikipedia.org/wiki/Damping>>.



33. K.O. Genc, R. Gopalakrishnan, M.M. Kuklis, C.C. Maender, A.J. Rice, K.D. Bowersox, P.R. Cavanagh, (2010)

Foot forces during exercise on the International Space Station, Journal of Biomechanics, Volume 43, Issue 15, Pages 3020-3027, ISSN 0021-9290, 10.1016/j.jbiomech.2010.06.028.

(<http://www.sciencedirect.com/science/article/pii/S0021929010003647>)

34. Alan R. Hargens, Sara Richardson, (2009)

Cardiovascular adaptations, fluid shifts, and countermeasures related to space flight, Respiratory Physiology & Neurobiology, Volume 169, Supplement, Pages S30-S33, ISSN 1569-9048, 10.1016/j.resp.2009.07.005.

(<http://www.sciencedirect.com/science/article/pii/S1569904809001840>)

## **Patent Rights**

United States Patent entitled EXERCISE MACHINE FOR USE WITH LOWER BODY NEGATIVE PRESSURE BOX which application was filed in the United States Patent and Trademark Office on February 21, 2013, as application serial number 61/767,551